Differential impact of Dicer deficiency on microglia of the developing and adult brain

Diana Varol[1], Alexander Mildner[1], Thomas Blank[2], Anat Shemer[1], Neta Barashi[1], Simon Yona[1], Eyal David[1], Sigalit Boura-Halfon[1], Yifat Segal-Hayoun[1], Louise Chappell- Maor[1], Hadas Keren-Shaul[1], Eran Hornstein[3] Martin Fuhrmann[4], Ido Amit[1], Nicola Maggio[5], Marco Prinz[2, 6] and Steffen Jung[1]

Departments of [1] Immunology and [3] Molecular Genetics, The Weizmann Institute of Science, Rehovot, Israel
[2] Institute of Neuropathology, Freiburg University Medical Centre, Germany
[4] Neuroimmunology and Imaging, German Center for Neurodegenerative Diseases (DZNE), Bonn
[5] Department of Neurology, The Chaim Sheba Medical Center, Sackler Faculty of Medicine and Sagol School of Neuroscience, Tel Aviv University, Tel Aviv, Israel.
[6] BIOSS Centre for Biological Signalling Studies, University of Freiburg, Germany

*correspondence to:
Steffen Jung, PhD
Department of Immunology
The Weizmann Institute of Science
Rehovot 76100, Israel
Tel: 00972 8 934 2787
FAX: 00972 8 934 4141
e.mail: s.jung@weizmann.ac.il

Keywords: microglia, microRNAs, DNA repair, dicer

SUMMARY

Microglia seed the embryonic neuro-epithelium, expand and actively sculpt neuronal circuits in the developing CNS, but eventually adopt relative quiescence and ramified morphology in the adult. Here we probed the impact of post-transcriptional control by microRNAs (miRNAs) on microglial performance during development and adulthood by generating mice lacking microglial *dicer* expression at these distinct stages. Conditional Dicer ablation in adult microglia revealed that miRNAs were required to limit microglial responses to challenge. Specifically, following peripheral endotoxin exposure, Dicer-deficient microglia overexpressed pro-inflammatory cytokines and as a result, impaired hippocampal neuronal functions. In contrast, prenatal ablation resulted in spontaneous microglia activation and revealed Dicer involvement in DNA repair and preservation of genome integrity. Accordingly, Dicer-deficiency rendered otherwise radio-resistant microglia sensitive to gamma-irradiation. Collectively, the differential impact of the Dicer ablation on microglia of the developing and adult brain highlights the changes these cells undergo with time.

Highlights

- miRNAs curb activation of adult microglia following challenge
- Microglia hyper-activation results in acute impairment of hippocampal neuronal functions
- Proliferative Dicer-deficient microglia in the developing brain accumulate DNA damage
- Microglia of developing and adult brain are highly distinct

INTRODUCTION

Tissue macrophage compartments evolve locally and independent from each other alongside their organ microenvironment (Amit et al., 2016). They are hence intimately associated with their immediate surroundings and acquire, beyond their established generic function as immune sentinels, activities tailored to assist local tissue needs (Varol et al., 2015). Microglia are yolk sac-derived macrophages residing in brain and spinal cord, where they interact with neurons and other glial cells by constantly probing the parenchyma with dynamic extensions (Davalos et al., 2005; Nimmerjahn et al., 2005). Microglia actively contribute to synaptic pruning and microglial interactions with synaptic elements are affected by neuronal activity. This notion is supported by sustained neuronal phenotypes and functional deficits in neuronal connectivity in mice harboring microglia mutant for complement or CX_3CR1 chemokine receptors (Paolicelli et al., 2012; Schafer et al., 2012). Contributions of microglia to physiological brain function are further underlined by neuropsychiatric or neurologic disorders for which microglial dysfunctions seem to be disease-causing (Prinz and Priller, 2014), such as the *csf1r* mutation-associated hereditary diffuse leuko-encephalopathy with spheroids (HDLS) (Rademakers et al., 2012), as well as fronto-temporal dementia and Alzheimer's disease linked to genetic variations of Trem2 (Guerreiro and Hardy, 2013; Poliani et al., 2015; Wang et al., 2015).

Differentiation and tissue specific activation of macrophages require precise regulation of gene expression that is governed by epigenetic mechanisms, such as DNA methylation, histone modifications and chromatin structure (Amit et al., 2016). Expression signatures are further subject to post-transcriptional and post-translational regulation. A major established post-transcriptional filter comprises regulation by microRNAs (miRNAs), a family of endogenous small non-coding RNAs (ncRNAs), that shape gene expression under physiological and pathological conditions (Bartel, 2009). miRNAs are generated from hairpin structured pre-miRNA transcripts that are processed in the cytoplasm by the ribonuclease type III Dicer1 (Dicer) (Bernstein et al., 2003). Once mature, Dicer loads the ~22 nucleotide-long single-stranded miRNAs onto the RNA-induced silencing complex (RISC) that targets mRNAs, based on sequence complementarity between their 3' untranslated region (UTR) and the respective miRNAs (Guo et al., 2010) (Kim et al., 2009).

Here we investigated the role of miRNA-based post-transcriptional regulation in the maintenance of microglia identity and function. Specifically, we used

constitutive or inducible CX_3CR1 promoter-driven Cre recombinase combined with conditional *dicer* alleles to generate animals whose microglia lack Dicer and as a result, miRNAs and other Dicer-dependent small non-coding RNAs, either in adulthood, or starting with development.

We show that the absence of Dicer and its products, when introduced postnatally, led to a reduction of microglia abundance, but was largely compatible with microglial steady state performance. However, miRNAs were required to curb microglia activation following peripheral endotoxin encounter, when Dicer-deficient microglia of challenged mice overexpressed pro-inflammatory cytokines resulting in impairment of hippocampal synaptic transmission. In contrast, prenatal Dicer ablation caused spontaneous microglia activation and accumulation of DNA damage suggesting miRNA-independent Dicer functions. Highlighting Dicer requirement for DNA repair, Dicer-deficient microglia of both developing and adult brain became radio-sensitive. Collectively, the observed differential impact of the Dicer deficiency on microglia highlights the profound changes this cellular compartment undergoes with time.

RESULTS

Microglia display a distinct microRNA profile.

To investigate how miRNAs contribute to the establishment and maintenance of microglial identity, we profiled the miRNA repertoire of adult microglia and compared it to intestinal macrophages and liver Kupffer cells (KC), as representatives of peripheral tissue-resident macrophages **(Figure S1A)**. Among 160 miRNAs expressed by microglia, 76 were shared with either or both reference populations (**Figure 1A**, cluster II, III; **Figure S1C**), while 84 miRNAs were specific for microglia (cluster I**, Figure 1A, Figure S1B)**. The latter included miR-99a, miR-125b-5p and miR-342-3p, shown to be induced in cultured microglia by TGF (Butovsky et al., 2014), which was proposed to be part of the tissue imprint establishing microglia identity (Gosselin et al., 2014). The microglial miRNome further comprised miRNAs reported to control microglial activation following inflammation or injury, such as let-7c, let-7i and miR-181c (Banerjee et al., 2013; Zhang et al., 2012). Microglia moreover shared expression of other inflammation-associated miRNAs, such as miR-146a-5p (Saba et al., 2012; Taganov et al., 2006) with colonic macrophages (Cluster III, **Figure 1A**) and let-7a-5p and let-7d-5p (Iliopoulos et al., 2009) with both KC and

intestinal macrophages (**Figure S1C**). Overall, this establishes that adult steady-state microglia display a specific miRNA signature (**Figure 1B**), including miRNAs associated with tissue imprint and control of cell activation.

To determine whether posttranscriptional control by miRNAs contributes to adult microglia maintenance and function, we generated mice lacking Dicer in these cells. Specifically, we crossed *dicer^{fl}* mice (Harfe et al., 2005) with *cx3cr1^{CreER}* animals, in which *Cre* recombinase activity can be induced in microglia and selected other tissue macrophages by tamoxifen (TAM) administration (Goldmann et al., 2016; 2013; Yona et al., 2013). Dicer-deficient mice die *in utero*, whereas heterozygote mutants are viable without an overt phenotype (Bernstein et al., 2003). To increase mutagenesis efficiency, we hence performed this study on a *cx3cr1^{CreER}:dicer$^{fl/-}$* background.

Cx3cr1^{CreER}:dicer$^{fl/-}$ mice were treated with five consecutive TAM injections at the age of 4 weeks (**Figure 1C**). PCR analysis of genomic DNA isolated from sorted microglia of animals six weeks post TAM treatment confirmed efficient rearrangement of the 'floxed' alleles (**Figure 1D**). More importantly, qRT-PCR analysis at the same time point revealed the essential absence of miRNAs from mutant microglia (**Figure 1E**). Maturation of miR451a-5p, which is Dicer-independent, but relies on the endonuclease Argonaute 2 (Ago2) (Cheloufi et al., 2010) was unaffected, indicating that the observed miRNA reduction is specific to the *dicer* loss.

Dicer is largely dispensable for steady state maintenance of adult microglia.

Cx3cr1^{CreER}:dicer$^{fl/-}$ mice harboring miRNA-depleted microglia did not develop any overt phenotype, up to 3 months following TAM-treatment. To examine the effect of the miRNA deficiency on microglia homeostasis, including cell numbers and morphology, we performed a histological analysis on brains of the animals. *Cx3cr1^{CreER}:dicer$^{fl/-}$* mice displayed, as compared to littermate controls, a significant reduction in microglial numbers in cortex and hippocampus **(Figure 2A, B)**. Ramified morphology can be taken as proxy for a resting state of microglia (Harry, 2013; Lawson et al., 1992). Three-dimensional morphometric measurements of *cx3cr1^{CreER}:dicer$^{fl/-}$* microglia revealed no significant changes in length of processes, numbers of segments and branch points, though filament dendrite volumes were slightly increased (**Figure 2C, D**). To test motility and tissue surveillance activity of Dicer-deficient microglia *in vivo,* we introduced a conditional reporter allele into the

animals and monitored fine microglial processes in the intact brain of living mice (Fuhrmann et al., 2010). Analysis of microglial process dynamics revealed only a very subtle, though consistent, reduction of the process turnover rate in the *cx3cr1^{CreER}:dicer$^{fl/-}$* mice **(Figure S2**). Taken together, miRNA absence from adult microglia did not result in overt spontaneous *in situ* activation of the cells, although it affected microglia numbers.

The specific miRNome of adult microglia suggests that miRNAs modulate the steady state microglia transcriptome. Accordingly, comparative RNA-seq analysis of microglia isolated from TAM-treated *cx3cr1^{CreER}:dicer$^{fl/-}$* mice and littermate controls revealed 183 up-regulated and 128 down-regulated genes (with >1.5 fold change (0.6 log2 ratio) and P<0.05; **Figure 3A**). Functional categorization by ingenuity pathway analysis (IPA) for top canonical pathways (P<0.05, Abs (Z score)<0.05) and the DAVID bioinformatics database (Dennis et al., 2003) for Gene Ontology annotation of enriched biological processes (P<0.05) showed altered genes to be associated with cell adhesion and motility, among others **(Figure S3A, B)**. The "cell adhesion" category included *cd47*, *cd34*, *nid2* and *scarb1 and the* "*integrin signaling*" category comprised *itga6*, *itgaV* and *itgb3 (Cd61)* **(Figure 3B)**. Increased expression of CD34 and CD61 was confirmed by flow cytometry **(Figure 3C)***.* In line with the notion that miRNAs fine-tune transcriptomes (O'Connell et al., 2012), overall changes were subtle (only 143 genes with at least 2 fold change, P<0.05). Collectively, these data indicate that miRNA absence from adult microglia does not result in their activation.

Dicer deficient microglia are hyper-responsive to systemic LPS challenge. To explore whether miRNA absence affects microglial responses to inflammatory stimuli, we challenged *cx3cr1^{CreER}:dicer$^{fl/-}$* mice and controls with the bacterial endotoxin lipopolysaccharide (LPS). Specifically, animals were treated with a single intra-peritoneal (*i.p*.) LPS injection, brain microglia were isolated six hours later and subjected to RNA-seq analysis. Both control and miRNA-deficient microglia responded robustly **(Figure 4A, Figure S4A)**. 351 genes were found similarly induced in both control and mutant microglia (cluster I, II), including *myd88*, *tlr2, cd14, trem1* and *tnf*, while 172 genes showed less induction in mutant cells (cluster III). Finally, miRNA-deficient microglia displayed prominent hyper-induction of 195 genes (cluster IV), which comprised IL1β-associated genes (*il1b, il18rap*), the ECM-

related pro-inflammatory gene fibronectin 1 gene (*fn1*), chemokines (*ccl17, ccl21*), as well as co-stimulatory molecules (*cd40, cd74*) **(Figure 4A, B)**. Overexpression of the pro-inflammatory cytokines *Il1b* and *Il6*, as well as *il18rap* and *fn1* by mutant microglia post systemic LPS challenge was validated by qRT-PCR analysis **(Figure 4C, S4D)**. Increased surface expression of CD40 and CD11b (*itgam*) by mutant cells was confirmed by flow cytometric analysis and was evident both in steady state and following LPS exposure **(Figure 4D)**. Confirming the general role of miRNAs in curbing microglia activation, microglia was also found hyper-responsive to a systemic poly I:C challenge (**Figure S4D)**.

To identify miRNAs, whose absence might be responsible for the transcriptome dysregulation in Dicer-deficient microglia following the LPS challenge, we aligned the upregulated genes with a list of conserved miRNA targets (**Figure S4B, C**). 10 miRNAs passed the significance threshold of the two tests we used (**Figure S4B, C**). Interestingly, six of these miRNAs were expressed in steady state microglia **(Figure 1A, Figure S1B, C, Figure 4E)**. miR-126a-3p, on the other hand, a miRNA absent from the steady state microglia, was found induced following the LPS challenge (**Figure 4F**).

Taken together, these data establish that Dicer-deficient microglia hyper-respond to a peripheral LPS challenge, corroborating the critical role of miRNAs in controlling inflammation.

Hyper-active dicer deficient microglia acutely impair hippocampal neuronal functions.

Systemic endotoxin challenge was shown to transiently impair the response of hippocampal neurons to repeated synapse stimulation (Maggio et al., 2013; Strehl et al., 2014; Vereker et al., 2000) (Chen et al., 2008; Kohman and Rhodes, 2013). Pro-inflammatory cytokines, such as TNF and IL1β, affect glutamate receptor activity on neurons in the CA1 area of the hippocampus (Riazi et al., 2015). However specific microglia contributions to this phenomenon of impaired hippocampal long-term potentiation (LTP) are not yet established.

Dicer-deficient hippocampal microglia displayed a hyper-activation response that largely overlapped with the response of whole brain mutant microglia, including increased expression of *il1b* and co-stimulatory molecules **(Figure 5A, B; Figure 4A,**

Figure S5A, B, Table S1). As previously shown (Vereker et al., 2000), LPS challenge led to induction of IL1β protein in the hippocampus (**Figure 5C**). Moreover, hyperactivation of Dicer-deficient microglia was reflected in increased pro-IL1β protein expression six hours following the LPS treatment **(Figure 5D**). To test a potential impact of the hyperactive Dicer-deficient microglia on neuronal fitness, we performed extracellular recordings on acute slices prepared from dorsal hippocampi of the animals (Strehl et al., 2014) and examined LTP 12 and 24 hr post LPS stimulus **(Figure 5E)**. *Cx3cr1^{CreER}:dicer$^{fl/-}$* mice presented unaltered baseline synaptic transmission and excitatory synaptic strength, as compared to controls **(Figure S5C)**. LTP of all mice was reduced by 12 hr post LPS challenge, however the neuronal response of the TAM-treated mutant *cx3cr1^{CreER}:dicer$^{fl/-}$* animals was significantly more affected **(Figure 5F, Figure S5D)**. In line with the reported transient nature of the effect, control mice displayed partial LTP recovery by 24 hr; *cx3cr1^{CreER}:dicer$^{fl/-}$* animals however showed persistent LTP reduction **(Figure 5F, Figure S5D)**. Overall, these results suggest that hyper-activation of Dicer-deficient microglia after peripheral LPS challenge results in a prolonged hippocampal LTP impairment and acutely affect neuronal circuits.

Prenatal Dicer mutagenesis induces DNA damage in newborn microglia and renders microglia radio-sensitive.

Unlike in the adult, microglia in the developing CNS are highly proliferative, migratory and display profound phagocytic activity (Harry, 2013; Orłowski et al., 2003). This is in line with the critical contributions of embryonic microglia to the establishment and maturation of neuronal circuits (Paolicelli et al., 2012; Schafer et al., 2012; Squarzoni et al., 2014). Embryonic (E14) and newborn (P0) microglia display transcriptomes that are distinct from adult microglia, with one fifth of the expression signature specific for the respective stage (**Figure 6A, B**), see also (Kierdorf et al., 2013; Mass et al., 2016; Matcovitch-Natan et al., 2016). Establishment of 'relative quiescence' in adult microglia was proposed to be related to their expression of the zinc finger transcriptional repressor Sall1 (Buttgereit et al., 2016). In line with their reported activity, E14 and P0 microglia expressed cell cycle-associated genes, including *ccnb1, cdc25a* and *cdk1.* Moreover E14 and P0 microglia displayed signs of an oxidative stress response (*cdc34, ftl1, hmox1, prdx1)* (cluster II) suggesting ROS

production, as also supported by high NADPH oxidase (Nox2) expression (*cybb*) of E14 microglia (cluster I, **Fig. 6A**).

Given the functional differences between neonatal and adult microglia, we decided to probe the effect of the Dicer deficiency on pre- and neonatal microglia by generating *cx3cr1*^{Cre}:*dicer*$^{fl/fl}$ mice (Harfe et al., 2005; Yona et al., 2013). In these animals, Cre recombinase is expressed at day E7.5 in primitive CX_3CR1^+ yolk sac macrophages that give rise to microglia (Bertrand et al., 2005; Ginhoux et al., 2010) **Figure 6C**). Dicer and miRNA absence in microglia of adult six week old *cx3cr1*^{Cre}:*dicer*$^{fl/fl}$ mice was validated by qRT-PCR analysis (**Figure 6D**). Gene expression profiling at P0 revealed that Dicer-deficient cells displayed 159 up- and 256 down-regulated genes (out of a total of 8545 genes), as compared to controls (**Figure 6E**). Dicer-deficient P0 microglia showed prominent induction of the "*DNA damage response*" pathway **(Figure S6A)**, as manifested by up-regulation of *cdkn1a*, *cdkn2d*, *ddit4* and *dst* **(Figure 6F, G)***.* Moreover, concomitant reduction of the "*cyclins and cell cycle*" pathway, including *ccnb1, cdk4* and *mcm2* **(Figure 6F, Figure S6A)**, suggested that mutant microglia respond to accumulated DNA damage by cell cycle arrest (Zhou and Elledge, 2000). Indeed, EDU labeling and Ki67 staining revealed that the frequency of proliferating newborn microglia was significantly reduced in *cx3cr1*^{Cre}:*dicer*$^{fl/fl}$ mice, as compared to littermate controls (**Figure 6H, Figure S6B, C)**.

To directly examine DNA integrity of Dicer-deficient microglia, we performed a gel electrophoresis-based 'comet assay' that allows visualization of single and double strand DNA breaks on single cell level (Olive and Banáth, 2006). As shown in **Figure 7A**, microglia sorted from brains of newborn *cx3cr1*^{Cre}:*dicer*$^{fl/fl}$ mice, but not littermate controls, displayed significant DNA damage. This suggested that newborn Dicer-deficient microglia are unable to repair endogenous DNA damage potentially resulting from their prominent replication or ROS production (McKinnon, 2013; Zhou and Elledge, 2000), a phenotype that might relate to miRNA-independent Dicer activity in DNA repair (Francia et al., 2012; Wei et al., 2012).

Microglia are characterized by profound resistance to ionizing radiation (Mildner et al., 2007). To test if lack of Dicer and the associated impaired DNA repair renders these cells radio-sensitive, we irradiated *cx3cr1*^{Cre}:*dicer*$^{fl/fl}$ and control mice (950 rad) and analyzed the frequency of apoptotic microglial cells. Irradiated Dicer-deficient microglia comprised significantly more late apoptotic events than controls,

indicating increased radio-sensitivity **(Figure 7B, Figure S7A)**. Next, we lethally irradiated *cx3cr1^{Cre}:dicer$^{fl/fl}$* mice and controls at P0 or at four weeks of age and reconstituted them with bone marrow (BM) isolated from *cx3cr1^{gfp}* reporter animals. In line with microglial radio-resistance, brain macrophage compartments of control chimeras showed only minor engraftment, even when irradiated newborns were used as recipients **(Figure 7C, D)**. In stark contrast, Dicer-deficient microglia were quantitatively replaced by *cx3cr1^{gfp}* BM-derived cells in the chimeric mice. Importantly, radiosensitivity was a general feature of Dicer-deficient microglia. Thus, also adult TAM-treated *cx3cr1^{CreER}:dicer$^{fl/-}$* animals, when irradiated and engrafted with WT BM, showed significant replacement of their microglia by graft-derived macrophages **(Figure S7B)**. Notably though, WT BM engraftment efficiency declined with time in these mice **(Figure S7B)**. This indicates a progressive loss of mutant microglia in these animals as also highlighted by the declining frequency of dicer null allele in sorted *cx3cr1^{CreER}:dicer$^{fl/-}$* microglia over time **(Figure S7C)**. Dicer-deficient microglia probably have a disadvantage over residual dicer-proficient cells, which were shown to harbor profound expansion potential (Bruttger et al., 2015). Collectively, these data establish a critical role of Dicer in microglial repair of endogenously or exogenously induced DNA damage.

Finally, we found adult *cx3cr1^{Cre}:dicer$^{fl/fl}$* - but not TAM-treated *cx3cr1^{CreER}:dicer$^{fl/-}$* mice - to display sporadic pathologies, including impaired dental growth (data not shown), likely due to the impairment of other tissue macrophage populations in these animals. Indeed, the dicer deficiency resulted in depletion of selected additional cells, such as Langerhans' cells (LC), as earlier reported (Turner et al., 2011) and dendritic epidermal T cells (DETC) (**Figure S8**). Microglia of adult *cx3cr1^{Cre}:dicer$^{fl/fl}$* mice exhibited an activated morphology characterized by an amoeboid shape and increased cell body size, as compared to littermate controls (**Figure S9A, B, C**). Microglia densities measured in the cerebellum, cortex and spinal cord were, however, largely unaltered (**Figure S9D**). By the age of six to eight weeks, all *cx3cr1^{Cre}:dicer$^{fl/fl}$* animals developed a motoric hind leg deficiency (**Figure S9E-G**). Prenatal dicer ablation and absence of regulatory miRNAs or other Dicer-dependent ncRNAs in developing microglia could thus have a long-term effect associated with CNS dysfunction, although the mechanism underlying this phenomenon, and its direct link to the microglia impairment remain to be elucidated.

DISCUSSION

Recent studies have highlighted the impact of the local tissue environment on macrophage identities; however, mechanisms that establish and maintain specific expression signatures remain incompletely understood (Amit et al., 2016). Here, we investigated the role of Dicer and Dicer-dependent ncRNAs, such as miRNAs, in microglia biology. Specifically, we used two complementary experimental systems to ablate Dicer either during microglia development or in adulthood. We show that the same genetic perturbation, i.e. ablation of *dicer*, has a differential impact on microglia in the adult and developing brain, since microglia are in different functional states in these time windows.

Despite the characteristic miRNome of adult microglia and the notion that lack of miRNAs results in increased protein expression noise (Schmiedel et al., 2015), we found Dicer and its products largely dispensable for the maintenance of adult microglial function under physiological conditions, including their characteristic morphology and extension dynamics. Specifically, Dicer deficient adult microglia did not show signs of spontaneous activation according to morphology and expression profile, however they did display a reduced tissue density and were in steady state progressively, albeit slowly, out-competed by rare Dicer-proficient cells.

MiRNAs have an established role in controlling cellular activation (O'Connell et al., 2012). Accordingly, miRNA absence from microglia resulted in profound hyper-activation of these cells following peripheral challenges, including LPS and poly I:C. The microglial steady state miRNome comprises miRNAs predicted to target 3'UTRs of pro-inflammatory genes, such as *il1b*, including miRNA-331-3p and miRNA-125b-5p. Moreover, microglia challenge results in induction of additional miRNAs that shape pro-inflammatory responses, including miR-155 miR-223, miR-218 and miR-194 (Butovsky et al., 2012), as well as miRNA-126a-3p, shown in this study. The latter targets the inflammatory response genes *nfkb2* and *slc11a2* (Cellier et al., 2007; Mancino et al., 2013), which we found increased in the Dicer mutant microglia following LPS challenge. The observed challenge-induced hyper activation in Dicer-deficient microglia likely results from the combined absence of steady state and induced anti-inflammatory miRNAs, as also indicated by our bio-informatic analyses. Moreover, in addition to miRNA maturation, Dicer has been implied in the processing of other ncRNAs involved in regulating the immune response. The latter include toxic Alu/B1/B2 ncRNAs (Kaneko et al., 2011), which accumulate in Dicer absence, and

activate the NLRP3 inflammasome (Gelfand et al., 2015). Such miRNA-independent mechanisms might contribute to the fact that microglia of *cx3cr1^{Cre}:dicer$^{fl/fl}$* and *cx3cr1^{CreER}:dicer$^{fl/-}$* mice show hyper-activation, either spontaneous, or following challenge.

Peripheral endotoxin challenge results in a neuro-inflammatory response and transient impairment of hippocampal LTP (Chen et al., 2008; Kohman and Rhodes, 2013). More specifically, pro-inflammatory cytokines, such as TNF and IL1β, were shown to affect glutamate receptors activity in the CA1 area of the hippocampus (Riazi et al., 2015); however the specific effect of microglia activation on the stimulation of CA1 pyramidal neurons and the resulting LTP response *in vivo* was not examined so far. Here we show that TAM-treated *cx3cr1^{CreER}:dicer$^{fl/-}$* mice displayed, as compared to littermate controls, a significantly weakened hippocampal neuron response to repeated synapse stimulation, as well as delayed recovery. *Cx3cr1^{CreER}:dicer$^{fl/-}$* mice might thus provide a valuable model to study the interplay of hyper-activated microglia with hippocampal astrocytes and neurons in the context of the LTP response, and define molecular parameters of their cellular crosstalk, including the role of TNF (Habbas et al., 2015). Of note, in *cx3cr1^{CreER}:dicer$^{fl/-}$* mice also non-parenchymal CNS macrophages are targeted (Goldmann et al., 2016). Although we show an effect of the dicer mutation in isolated microglia, we hence cannot rule out that mutagenesis of these populations contributes to the LTP impairment. Future studies should also address the impact of microglia hyperactivation on cognitive and associative memory characteristics and behavioral comorbidities seen in patients.

Dicer promotes cell survival and its absence can result in cell death, as shown for neurons, glia and immune cells (Kim et al., 2009; Koralov et al., 2008; Kuipers et al., 2010; Schaefer et al., 2007; Tao et al., 2011). Accordingly, also *cx3cr1^{Cre}: dicer$^{fl/fl}$* mice lacked selective cell populations, for instance in the epidermis, that express CX_3CR1 either during development (LC) or upon maturation (DTEC). Microglia tissue density and motility were reduced in both hippocampus and cortex of *Cx3cr1^{CreER}: dicer$^{fl/fl}$* mice, as compared with WT mice, indicating an effect on microglia network connectivity and survival. Moreover, in the TAM-treated *cx3cr1^{CreER}: dicer$^{fl/-}$* mice, mutant cells were over time slowly outcompeted by Dicer-proficient microglia. Dicer-dependent cell survival is likely related to a critical role of Dicer in DNA repair and

preservation of genome integrity (Swahari et al., 2016), including in response to γ irradiation induced DNA damage (Francia et al., 2012; Wei et al., 2012). In support of this notion, the Dicer deficiency rendered the otherwise radio-resistant microglia radio-sensitive, both at the perinatal and adult stages, as demonstrated in both the *cx3cr1*^{Cre}*:dicer*$^{fl/fl}$ and TAM-induced *cx3cr1*^{CreER}*:dicer*$^{fl/-}$ mice. Dicer deficiency in development, a stage where the microglia are highly proliferative and active and thus exposed to endogenous genotoxic stress, resulted in a prominent accumulation of DNA damage. In contrast, the need for Dicer in DNA repair in the more quiescent adult microglia was revealed when the cells were damaged by external manipulation, i.e. □□□□irradiation. Future studies should investigate the long-term impact of the DNA repair defect on microglial genome integrity and the establishment of microglial senescence.

Adult *cx3cr1*^{Cre}*: dicer*^{flfl} mice develop a significant, though non-progressive Amyotrophic Lateral Sclerosis (ALS)-like motoric hind leg deficiency. The exact cause of this phenomenon remains unclear. Notably, when combined with certain 'floxed' reporter alleles, adult *cx3cr1*^{Cre} mice display rearrangements in neurons (Varol et al., *in preparation*). As adult neurons do not express CX_3CR1, this is likely due to a yet undefined narrow and transient window of CX_3CR1 promoter activity during their development. We can therefore not formally exclude that the delayed motor neuron defect in these mice results from Dicer impairment in neurons. Alternatively, the profound cell-intrinsic impairment of the Dicer-ablated microglia in the critical time window of CNS development might have a permanent impact on the integrity of neuronal circuits, which precipitates in the delayed pathology.

Collectively, we show the requirement of Dicer and miRNAs for microglia function and maintenance during development and adulthood. Perinatal absence of dicer impaired proliferative expansion and DNA integrity of microglia, and caused spontaneous hyper-activation. Microglial Dicer ablation in adulthood did not cause spontaneous activation of microglia in steady state, but resulted in hyper-microglial responsiveness to challenge and as a consequence, acute impairment of neuronal circuitries. This differential impact of the Dicer deficiency highlights the prominent changes microglia undergo with time from the developing to the adult brain.

EXPERIMENTAL PROCEDURES

Mice

The following newborn (P0) - to 24-week-old mice were used**:** C57BL/6 (CD45.2); B6.SJL-*Ptprca Pep3b*/Boyj (Jackson Laboratories) (CD45.1); *cx3cr1*$^{gfp/+}$ mice (JAX stock 005582 B6.129P-Cx3cr1tm1Litt/J (Jung et al., 2000); *cx3cr1*^{Cre} *(*JAX stock 025524 B6J.B6N(Cg)-Cx3cr1tm1.1(cre)Jung/J) *and cx3cr1*^{CreER} mice (JAX stock 020940 B6.129P2(C)-Cx3cr1tm2.1(cre/ERT2)Jung/J) (Yona et al., 2013); *dicer*$^{fl/fl}$ mice (B6.Cg-*Dicer1tm1Bdh*/J, Jackson laboratories) (Harfe et al., 2005); and Rosa-26-YFP mice (B6.129X1-*Gt(ROSA)26Sortm1(EYFP)Cos*/J) (Srinivas et al., 2001). All animals were on C57BL/6 background and maintained in specific pathogen-free (SPF) conditions and handled according to protocols approved by the Weizmann Institute Animal Care Committee as per international guidelines.

Generation of bone marrow (BM) chimeras

BM chimera animals were lethally irradiated (950 rad) and reconstituted the following day via *i.v.* injection of 5X10^6 donor whole BM cells per mouse. Chimeras analysis was performed six weeks following the BM transfer.

Animal treatments

To induce gene recombination in CreER transgenic mice, tamoxifen (TAM) was dissolved in warm corn oil (Sigma) and administered orally via gavage (Kiermayer et al., 2007) for five consecutive times. All animals were TAM-treated first at 4 weeks of age. Each oral application was of 10 mg at a concentration of 10 mg/100 □l. Mice were examined at least 6 weeks following treatment, unless indicated differently.

For LPS treatment mice were either injected intraperitoneally (*i.p*.) with a single dose of LPS [1 mg/kg; ≥500,000 (endotoxin units)/mg; E. coli 0111:B4; L4130 Sigma], the same volume of vehicle solution (PBS), or non-treated. For poly I:C treatment mice were either injected i.p with a single dose of poly I:C [20 mg/Kg; P1530 sigma], the same volume of vehicle solution (PBS), or non-treated.

Histology

Following paraformaldehyde (PFA) fixation (48hr in 4 degrees), brain and spinal chord (SC) were taken for frozen and paraffin sections, respectively. For frozen

sections, following incubation in PFA, tissues were equilibrated with 30% (wt/ vol) sucrose solution for 48 hr. Subsequently, samples were snap frozen in O.C.T (Tissue-Tek) by isopentane (Sigma) previously cooled with liquid nitrogen, and sectioned with a cryostat into 12 μm thick sections. Sections were stained with Iba1 (Wako, 019-19741, 1:150), CD68 (Biolegend, FA-11, 1:100) and Hoechst (vector). For paraffin sections, following incubation in PFA, tissues were embedded in paraffin, serially sectioned and stained after antigen retrieval with Iba1 (Wako, 019-19741, 1:150).

3D reconstruction of microglia

30-μm parasagittal cryo sections from adult brain tissue were stained with anti-Iba-1 (cat. no. 019-19741, Wako) for 48 hr (dilution 1:500 at 4 °C), followed by Alexa Fluor 568–conjugated secondary antibody (cat. no. A11011, Life technologies), which was added at a dilution of 1:500 overnight at 4 °C. Nuclei were counterstained with DAPI. Imaging was performed on an Olympus Fluoview 1000 confocal laser scanning microscope (Olympus) using a 20Å~ 0.95 NA objective. Z stacks performed with 1.14-mm steps in z direction, 1,024 Å~ 1,024 pixel resolution were recorded and analyzed using IMARIS software (Bitplane). Three cortical cells were reconstructed per analyzed mouse.

Surgery and Two photon *in vivo* imaging

A cranial window over the right cortical hemisphere was installed as previously described (Fuhrmann et al., 2010). Mice were anaesthetized with an intraperitoneal (*i.p.*) injection of ketamine/xylazin (0.13/0.01 mg/g body weight). Additionally, dexamethasone (0.02 ml at 4 mg/ml) was *i.p*. injected immediately before surgery to prevent swelling of the brain. A small incision was made to the skin over the right part of the skull. The skull was exposed and a circular piece of the skull (4 mm diameter) was removed using a dental drill (Schick-Technikmaster C1; Pluradent, Offenbach, Germany). A sterilized circular glass cover-slip (4 mm diameter) was inserted into the hole and fixed using dental acrylic (Cyano-Veneer fast; Heinrich Schein Dental Depot, Munich, Germany). Next to the cranial window a small metal bar was glued containing a winding for fixation of the mouse in a stereotactic frame under the microscope. After surgery, mice were placed in the custom made stereotactic frame

under the microscope (TrimScope II, LaVision Biotech, Germany) and supported by a heating plate to maintain the body temperature at 37°C. A 16X NA0.8 water immersion objective with a working distance of 3 mm (Nikon, Germany) was used to acquire images in vivo. YFP-fluorescent microglia were excited with a two-photon laser (Cameleon Ultra II, Coherent) at a wavelength of 920 nm with a maximum output power of 50mW to prevent photo damage. YFP emission was filtered with a bandpass filter (535-580 nm) and detected with highly sensitive gallium arsenide phosphide (GaAsP)-detector. Image stacks (400 x 400 x 300 µm) with a pixel size of 0.39 µm/pixel and a z-spacing of 3 µm were acquired every 5 minutes for a period of 40 minutes. At the end of the experiment, mice were sacrificed and the brains were removed for further processing.

Live imaging Analysis

The acquired z-stacks were median filtered and average intensity projections were performed of 30 µm spanning stacks in z-dimension. The average intensity projected time-series were registered using the TurboReg plugin in FIJI (ImageJ). Two images of subsequent time-points were overlaid and the precursor images were pseudo-colored in green and the successor images in magenta. In these pseudo-colored images we measured the area of gained (green) and lost (magenta) microglial processes. The turnover rate (TOR) of microglial processes was calculated as the sum area of gained and lost processes, divided by the whole area occupied by the microglia cell in percent.

Microglia isolation procedures

For isolation of adult microglia, prior to tissue collection, mice were perfused with phosphate buffered saline (PBS) via the heart left ventricle. Brain and spinal cord were dissected, crudely homogenized by pipetting and incubated for 15 min at 37 °C in a 1 ml HBSS solution containing 2% BSA, 1 mg/ml Collagenase D (Sigma) and 1 mg/ml DNase1 (Sigma). Next the homogenate was filtered through a 100 µm mesh, washed with cold PBS-/- and centrifuged at 1400 RPM, at 4°C, for 5 min. For the enrichment of microglia, the cell pellet was re-suspended with a 40% percoll solution and centrifuged at 2200 RPM, no acceleration and breaks, at 22 °C for 20 min. Next, the cell pellet was taken for antibody (Ab) labeling and flow-cytometry analysis. For

isolation of embryonic and newborn microglia, brain was gently pulled out and separated from the meninges, next the brain was grossly dissected and put for homogenization using gentleMACS tubes (Miltenyi, Bergisch Gladbach). For the enrichment of microglia, cell pellet was resuspended in a 40%/80% percoll solution and centrifuged at 2200 RPM, no acceleration and breaks, 22 °C for 20 min. The gradient interphase was collected, washed with cold PBS (1:10 ratio) and centrifuged at 1400 RPM, at 4 °C, for 5 min. Next, the cell pellet was taken for Ab labeling and flow-cytometry analysis.

Flow cytometry

Cells were stained with primary antibodies directed against CD11b (M1/70), CD45 (30-F11), CD45.1 (A20), CD45.2 (104), Ly6C (AL-21), LY6G (1A8), MHC class II (2G9), CD86 (GL-1), CD64 (X54-5/7.1) F4/80 (Cl:A3-1) CD11c (N418), CD40 (HM40-3), CD34 (MEC-14.7), CD61 (2C9.G2 (HMβ3-1)), AnnexinV - all Biolegend, San Diego, CA, USA, KI67 (SolA15; eBioscience, San-Diego, CA, USA) and 7AAD (BD, Erembodegem, Belgium). Following incubation with the surface Abs at 4 °C for 15 min, Cells were washed and analyzed using a FACSFortessa or for sorting with a FACSAriaIII (BD, Erembodegem, Belgium) flow cytometer. In the case of KI67, following surface staining, cells were fixed and permeabilized (FixPerm kit, BD) for the intracellular labeling of Ki67. Viable cells were gated by forward and side scatter pattern. Data were acquired with FACSdiva software (Becton Dickinson). Post-acquisition analysis was performed using FlowJo software (Tree Star, Inc.).

EDU labeling

To measure P0 microglia proliferation, 1.5 mg/300μl (50mg/Kg) of thymidine analogue, 5 ethynyl-29-deoxyuridine (EdU) (Invitrogen) diluted in PBS supplemented with 1:500 DMSO was *i.p* injected twice with a three hours difference between injections to the pregnant mother at E19. At E20 (P0) the brains were dissected and homogenized using the gentle MACS dispomix tubes (Miltenyi, Bergisch Gladbach). Next, brain cell suspension was enriched with a percoll gradient and stained with surface markers as described above. Following surface labeling, cells were fixed and permeabilized, followed by a chemical labeling of the incorporated EdU using the EdU staining kit according to manufacturer's instructions (Invitrogen).

Western blot

Tissues were extracted in RIPA buffer (20 mM Tris-HCl (pH 7.5), 150 mM NaCl, 1mM Na2EDTA, 1mM EGTA, 1% NP-40, 1% sodium deoxycholate, 2.5 mM sodium pyrophosphate, 1mM beta-glycerophosphate, 10mM NaF). Samples were separated by SDS-PAGE and immunoblotted using antibodies to IL1β (1:1000, R&D) and vincullin (1:250, hybridoma).

Agilent microRNA microarray

Total RNA from freshly sorted microglia, colonic macrophages, and liver macrophages was extracted using the miRNeasy Mini Kit (QIAGEN). RNA purity was assessed with a BioAnalyzer 2100 (Agilent Technologies). Expression levels of miRNAs were assayed by Agilent miRNA microarrays (Release 12.0 and 15.0), according to the manufacturer's protocols. Then, 100 ng of total RNA per sample (duplicates for each cell population from independent sorts) was labeled and hybridized according to the manufacturer's instructions. For K-Means clustering with Pearson correlation, only miRNAs with a ≥ 2-fold differential expression in at least 1 population were used. As a target prediction algorithm, TargetScanMouse 7.1 was applied.

RNA-seq

For RNA-seq 30,000 microglia cells per brain were sorted by FACS directly into a 1.7 ml micro-tube containing 50 µl lysis buffer (RNase-free H_2O, 0.2% Triton-X (Roth) and 0.4 U/µl RNasin (Promega). Next, the tube was centrifuged, snap frozen on dry ice and stored at –80 °C. RNA-seq library production, following sample preparation and analysis were carried out as described previously (Jaitin et al., 2014).

RNA-seq Processing and Analysis

RNA-seq reads were aligned the to the mouse reference genome (NCBI 37, mm9) using TopHat v2.0.13 with default parameters (Trapnell et al., 2009). Duplicate reads were filtered if they aligned to the same base and had identical UMIs. Expression levels were calculated and normalized for each sample to the total number of reads using HOMER software (http://homer.salk.edu) with the command

“analyzeRepeats.pl rna mm9 -d [sample files] -count 3utr -condenseGenes” (Heinz et al., 2010). For the RNA-seq analysis in Fig. 3, 4, 5 we focused on highly expressed genes with 2-fold differential over the noise (set as median of all expressing genes values). K-means clustering (matlab function kmeans) was used for k=8 in Figure 4, k=5 in Figure 6, and k=8 in Figure S5.

qRT-PCR

mRNA and miRNA expression quantification was performed on sorted brain microglia. In the case of sorted cells, 50-250 ng of total RNA isolated with miRNeasy micro-kit (Qiagen) were reverse transcribed with the miScript reverse transcription kit (QIAGEN) according to the manufacturer's instructions, resulting in reverse transcription of both mRNA and miRNAs. The miScript SYBR Green kit (QIAGEN) was used to detect amplification in an Applied Biosystems 7300 Real-Time PCR machine, for specific genes and miRNAs.

Electrophysiology in brain slices (LTP)

Extracellular recordings in acute slices prepared from dorsal hippocampus were performed as previously described (Maggio and Segal, 2007). Following anesthesia with ketamine/xylazine (0.13/0.01 mg/g body weight), animals were rapidly decapitated, the brain removed, and 400 μm slices prepared using a vibroslicer. Slices were incubated for 1.5 h in a humidified, carbonated (5% CO2 and 95% O2) gas atmosphere at 33 ± 1°C and perfused with artificial cerebrospinal fluid (ACSF) containing: 124mM NaCl, 2mM KCl, 26mM NaHCO3, 1.24mM KH2PO4, 2.5mM CaCl2, 2mM MgSO4, and 10mM glucose (pH 7.4) in a standard interface chamber. Recordings were made with a glass pipette containing 0.75M NaCl (4 MΩ) placed in stratum radiatum of CA1. Stimulation of Schaffer's collaterals was evoked using a pulse stimulator and delivered through a bipolar nichrome electrode. Input-output curves were run on each slice prior to beginning of each experiment. Before applying the tetanic stimulation, baseline values were recorded at a frequency of 0.033 Hz. LTP was induced by high-frequency stimulation (HFS) consisting of 100 pulses at twice the test intensity, delivered at a frequency of 100 Hz (1 s). Responses were digitized at 5 kHz and stored on a computer. Spike 2 software (Cambridge Electronic Design) was used for data acquisition.

Comet assay

The comet assay (Trevigen Inc., Gaithersburg, MD) was performed according to the manufacturer's protocol using neutral conditions. After lysis overnight at 4 °C, the slides were washed twice with 1X Tris-borate EDTA buffer solution, pH 8.3 (TBE) for 10 min each. The slides were placed in a horizontal electrophoresis chamber and covered with TBE buffer. Electrophoresis was carried out at the rate of 1.0 V/cm for 20 min. The slides were removed from the electrophoresis chamber, washed in deionized water for 5 min and immersed in ice cold 100% ethanol for 5 min. Subsequently, the slides were air dried, DNA was stained with 50 μl of SYBR Green I dye 1:10,000 in Tris–EDTA buffer, pH 7.5 for 20 min in the refrigerator and analyzed using an Olympus digital camera attached to an Olympus BX51 epifluorescence microscope.

Motoric activity assay

Home-cage locomotion. Mice were single-housed, and locomotive activity was examined automatically over a 48-h period using the InfraMot system (TSE Systems, GmbH).

Rotarod test. Mice were placed on an accelerating spinning wheel and their latency to fall was measured by an inframot beam. Mice were placed on a spinning wheel for five consecutive times, first two repetitions were considered training and last three repetitions were scored and averaged.

Hangwire test. Mice were attached to a wire by their forelimbs and their latency to grip wire with hind limbs was measured. Scoring equals the latency time, no grip or alternatively a fall was considered as "60 sec". Test was repeated 3 times with a 30 min gap between repetitions, scoring represented the average score of the three repetitions.

Statistics

Statistical analysis for differences between two or more groups was performed using GraphPad Prism (GraphPad Software, Version 6.0, La Jolla, USA). All data were tested for normality applying the Kolmogorov-Smirnov test. If normality was given, an unpaired t test was applied in the case of two groups comparison. In the case of

more then two groups comparison, a one-way Anova was performed followed by an unpaired t test for multiple comparisons.
For testing specific miRNAs targets enrichment within a data-set of upregulated genes, two tests were performed in parallel - a hypergeometric test counting the mutual genes between two data-sets followed by a measure for the randomality of the counts, and a gene-set–enrichment-analysis (using the GSEA software, broad institute, as described (Subramanian et al., 2005). Differences were considered significant when $P<0.05$.
For measuring similarity between whole brain microglia and hippocampal microglia, a Pearson correlation test was applied, using the Partek software.
To obtain unbiased data, experimental mice were all processed together by technicians and cell quantifications were performed blind by two scientists independently and separately.

SUPPLEMENTAL INFORMATION

Supplemental Information includes nine figures and one table, and can be found with this article online at .....

ACKNOWLEDGEMENTS

We would like to thank all members of the Jung laboratory for helpful discussion and the staff of the Weizmann Animal facility for the excellent care. We thank T. Paz-Elizur, U. Swain and V. Krizhanovsky (WIS), B. Stevens and D. Schafer for critical advice. This work was supported by the Israeli Science Foundation (887/11), teh MINERVA Foundation, the European Research Council (340345), and the Deutsche Forschungsgemeinschaft (CRC/TRR167 “NeuroMac” for SJ, IA, MP and TB).

FIGURE LEGENDS

Figure 1. Microglia display a distinct microRNA profile as compared to other tissue macrophages

(A) Heat map of miRNA expression of sorted microglia, liver and colon macrophages from 6 weeks old mice. Shown are miRNAs exhibiting an at least two fold change between any two distinct populations (235 miRNAs). Intensity values were log-transformed, normalized and centered, and genes were clustered by a Pearson correlation test, number of partition clusters was set to six. (2 replicates per cell type).
(B) Correlation matrix with Pearson correlation coefficient performed for all miRs expressed above background and displaying > 2-fold change between any two populations displayed in A.
(C) Scheme illustrating conditional TAM-induced mutagenesis using *cx3cr1^{CreER}:dicer$^{fl/-}$* mice.
(D) Representative genomic PCR analysis of sorted brain microglia of *cx3cr1^{CreER}:dicer$^{fl/-}$* mice and controls, six weeks after TAM treatment given at 4 weeks of age; data are a representative of 3 repeats .
(E) Diagram summarizing qRT-PCR analysis for expression of selected miRNAs in microglia sorted from brains of *cx3cr1^{CreER}:dicer$^{fl/-}$* and *cx3cr1^{CreER}:dicer$^{+/-}$* mice, six weeks after TAM treatment. Data are expressed as mean +/- SEM, statistically analyzed with student T test (*P<0.05, **P<0.01, NS P>0.05). n=3 per group.

Figure 2. Dicer-deficient adult microglia in steady state are affected in numbers, but not morphology

(A) Histological analysis of cortex and hippocampus of *cx3cr1^{CreER}:dicer$^{fl/-}$* mice and controls; Iba1 (red), Dapi (blue).
(B) Diagram summarizing microglia densities. Data are expressed as mean +/- SEM, statistically analyzed with student's T-test (*P<0.05, **P<0.01). *cx3cr1^{CreER}:dicer $^{+/-}$* (n=4), *cx3cr1^{CreER}:dicer$^{fl/-}$* (n=3).
(C) Representative three-dimensional reconstruction of cortical microglia morphology of *cx3cr1^{CreER}:dicer$^{fl/-}$* mice and controls.
(D) Imaris based automatic quantification of cell morphology. Each symbol represents an average of at least three cells measured in a specific tissue sample. Data are expressed as mean +/- SEM, statistically analyzed with student's T-test

(*P<0.05); n=3 per group.

Figure 3. Gene expression analysis of microglia of TAM-treated adult *cx3cr1^{CreER}:dicer$^{fl/-}$* mice

(A) Volcano plot of statistical significance (-log 10 p value) against log 2 ratio between *cx3cr1^{CreER}:dicer$^{fl/-}$* and *cx3cr1^{CreER}:dicer$^{+/-}$* control mice, based on the RNA-seq data. Significantly changed genes (at least 1.5 fold change (0.6 log2 ratio, P value <0.05) are represented by red symbols.
cx3cr1^{CreER}:dicer$^{fl/-}$ (n=3), *cx3cr1^{CreER}:dicer$^{+/-}$* (n=4).
(B) Heat map analysis showing log 2 transformed and standardized normalized read numbers of up-regulated genes associated with selected functional categorization presented in Figure S3A & B, based on ingenuity canonical pathway analysis and Go annotation analysis for biological process. *cx3cr1^{CreER}:dicer $^{+/-}$* mice (n=4); *cx3cr1^{CreER}:dicer$^{fl/-}$* mice (n=3).
(C) FACS analysis of microglial CD61 and CD34 surface expression levels (mean fluorescence intensity (MFI)), isolated from TAM-treated *cx3cr1^{CreER}:dicer$^{fl/-}$* mice (red) and controls (black). Data are expressed as mean +/- SEM, statistically analyzed with student's T-test (*P<0.05). n=3 per group.

Figure 4. Hyper-response of Dicer-deficient microglia to systemic LPS challenge

(A) Heat map analysis of mRNA profiles of microglia isolated from PBS or LPS treated *cx3cr1^{CreER}:dicer$^{fl/-}$* and control mice. Genes displayed represent a fold change of at least 2 between any two of the groups (1551 genes). Normalized read numbers were log-transformed and standardized. Genes were clustered by a Pearson correlation test and number of partition clusters was set to eight.
cx3cr1^{CreER}:dicer $^{+/-}$ PBS mice (n=3), *cx3cr1^{CreER}:dicer $^{+/-}$* LPS mice (n=4), *cx3cr1^{CreER}:dicer$^{fl/-}$* PBS mice (n=3) and *cx3cr1^{CreER}:dicer$^{fl/-}$* LPS mice (n=4).
(B) Examples of gene expression as identified in cluster IV (A). Shown are the mean sequence reads ± SEM.
(C) Graphical summary of qRT-PCR analysis showing relative quantities of mRNA for *il6* and *il1b* in microglia sorted 6hr following an *i.p* injection of either PBS or LPS of TAM-treated *cx3cr1^{CreER}:dicer$^{fl/-}$* and control mice. Data are expressed as mean ± SEM and statistically analyzed with one-way ANOVA for multiple comparisons

(*P<0.05, ***P<0.001). *cx3cr1^{CreER}:dicer $^{+/-}$* PBS (n=3), *cx3cr1^{CreER}:dicer$^{fl/-}$* PBS (n=3), *cx3cr1^{CreER}:dicer $^{+/-}$* LPS (n=8), *cx3cr1^{CreER}:dicer$^{fl/-}$* LPS (n=6).

(D) Graphical summary of surface expression of CD40 and CD11b on microglia isolated from *cx3cr1^{CreER}:dicer$^{fl/-}$* and control mice after *i.p* injection of either PBS or LPS. Data are expressed as mean fluorescence intensity ± SEM and statistically analyzed with one-way ANOVA for multiple comparisons (***P<0.001, ****P<0.0001). *cx3cr1^{CreER}:dicer $^{+/-}$* PBS (n=6), *cx3cr1^{CreER}:dicer$^{fl/-}$* PBS (n=2), *cx3cr1^{CreER}:dicer $^{+/-}$* 6hr LPS (n=5), *cx3cr1^{CreER}:dicer$^{fl/-}$* 6hr LPS (n=3), *cx3cr1^{CreER}:dicer$^{+/-}$* 24hr LPS (n=4), *cx3cr1^{CreER}:dicer$^{fl/-}$* 24hr LPS (n=3).

(E) Graphical summary of expression level of miRNAs predicted to target genes up-regulated in *cx3cr1^{CreER}:dicer$^{fl/-}$* microglia in response to LPS (see Table in Figure S4B, summarizing results obtained from two statistical tests used for miRNA prediction). Shown are mean intensity values for steady state expression of each miRNA in WT microglia, as measured in Agilent microarray (Figure 1A and Figure S1B, C); either expressed (filled bars); or absent in steady state (open bars).

(F) Expression level measured by qRT-PCR of miR142-3p and miR126-3p in WT microglia non-treated, 1hr, 2hr and 4hr after LPS *i.p* injection; miRNAs, expressed in steady state (filled bars); miRNAs, absent in steady state (open bars); data are expressed as mean ± SEM and statistically analyzed with Student's T test (*P<0.05). n=3 per group.

Figure 5. Hyper-active dicer deficient microglia impair hippocampal neuronal functions after LPS exposure

(A) Comparison of hippocampal and whole brain microglia log2 ratios between *cx3cr1^{CreER}:dicer$^{fl/-}$* and control mice gene expression 6hr post LPS *i.p* injection. Similarity of mutant microglia is indicated by Pearson correlation test (r=0.856); whole brain *cx3cr1^{CreER}:dicer $^{+/-}$* 6hr LPS (n=4), whole brain *cx3cr1^{CreER}:dicer$^{fl/-}$* 6hr LPS (n=4), hippocampal *cx3cr1^{CreER}:dicer $^{+/-}$* 6hr LPS (n=2), hippocampal *cx3cr1^{CreER}:dicer$^{fl/-}$* 24hr LPS (n=2). (see **Table S1** for detailed gene lists).

(B) Examples of gene expression for genes mutually up-regulated 6hr following LPS in both whole brain and hippocampus microglia from *cx3cr1^{CreER}:dicer$^{fl/-}$* mice compared to *cx3cr1^{CreER}:dicer $^{+/-}$* mice (shown in A). Shown are the mean sequence reads of hippocampal microglia ± SEM.

(C) Western blot analysis of hippocampal extracts of unchallenged and LPS-challenged *cx3cr1^{CreER}:dicer$^{fl/-}$* mice and littermate controls for expression of pro-IL1β protein, non-treated and 6 hr after LPS *i.p* injection. n=2 per group. Data are a representative of 2 repeats.

(D) Flow cytometric analysis of microglia isolated from unchallenged and LPS-challenged *cx3cr1^{CreER}:dicer$^{fl/-}$* mice and littermate controls for expression of pro-IL1β protein, 6 hrs after LPS *i.p* injection. Data are expressed as mean ± SEM and statistically analyzed with Student's T test (*P<0.05). *cx3cr1^{CreER}:dicer$^{fl/-}$*(n=4), *cx3cr1^{CreER}:dicer $^{+/-}$* (n=5).

(E) Graphical description of LTP measurement protocol. Stimulation of Schaffer's collaterals was evoked using a pulse stimulator and delivered through a bipolar nichrome electrode.

(F) LTP analysis on Schaffer collateral *cornu ammonis* 1 (CA1) region synapses probed in acute hippocampal slices isolated from either 12hr post PBS, 12hr post LPS or 24hr post LPS treated *cx3cr1^{CreER}:dicer$^{fl/-}$* mice and controls. Averaged EPSP are plotted versus time. Data are expressed as mean +/- SEM and statistically analyzed with two way ANOVA on time point 60 considering the type of treatment, genotype and the interaction between the two factors. (*P<0.05, **P<0.01 represent the significance of interaction). Representative traces at indicated times (a,b) are shown on top of each section. Upward arrows indicate the time of high-frequency stimulation (HFS). *cx3cr1^{CreER}:dicer $^{+/-}$* PBS, 12 hr, 24hr LPS (n=4 each); *cx3cr1^{CreER}:dicer$^{fl/-}$* PBS (n=3), 12 hr (n=4), 24hr LPS (n=4).

Of note, a repeat of this experiment, including an additional WT group is shown in **Figure S5D**.

Figure 6. DNA damage response and cell cycle arrest in newborn microglia after prenatal Dicer mutagenesis

(A) Heat map analysis of mRNA profiles of microglia sorted from embryonic day 14 (E14), newborns (P0) and adult (six weeks old) mice. Genes were filtered for at least 2 fold change between any couple of samples (2148 genes).

Normalized read numbers were log-transformed and standardized. Genes were clustered by Pearson correlation test, number of partition clusters was set to five. Prominent canonical pathways assigned by ingenuity pathway analysis are indicated

for each cluster. E14 (n=4), P0 (n=5), six weeks old (n=2).
(B) Venn diagram illustrating level of transcriptome overlap between prenatal (E14, red), newborn (P0, yellow) and adult microglia (six week, blue).
(C) Scheme illustrating E7.5 onset of constitutive microglial mutagenesis in *cx3cr1^{Cre}:dicer$^{fl/fl}$* mice.
(D) Summary of qRT-PCR analysis for expression of selected miRNAs in microglia sorted from brains of 6 weeks old *cx3cr1^{Cre}:dicer$^{fl/fl}$* and *dicer$^{fl/fl}$* mice. Data are represented as mean +/- SEM and statistically analyzed with student T test. (**P<0.01, NS P>0.05). *cx3cr1^{Cre}:dicer$^{fl/fl}$* (n=2), *dicer$^{fl/fl}$* mice (n=3).
(E) Volcano plot displaying statistical significance (-log 10 p value) against the log 2 ratio between sorted microglia isolated from *cx3cr1^{Cre}:dicer$^{fl/fl}$* and *dicer$^{fl/fl}$* mice based on RNA-seq data. Significantly changed genes (at least 2 fold change, P<0.05) are represented by the red symbols. *cx3cr1^{Cre}:dicer$^{fl/fl}$* (n=2), *dicer$^{fl/fl}$* mice (n=3).
(F) Heat map graphical display of genes of the DNA damage response checkpoint and cell cycle regulation categories, as defined by ingenuity pathway analysis (see also **Figure S6A**) in microglia isolated from *cx3cr1^{Cre}:dicer$^{fl/fl}$* and *dicer$^{fl/fl}$* mice. Shown are the standardized log2 transformed read numbers of significantly changed genes (at least 2 fold change, P<0.05). *cx3cr1^{Cre}:dicer$^{fl/fl}$* (n=2), *dicer$^{fl/fl}$* mice (n=3).
(G) Graphical summary of qRT-PCR analysis for *cdkn1a* expression (encoding p21). Data are expressed as mean ± SEM and statistically analyzed with Student's T test (*P<0.05); n=3 per group.
(H) EDU flow cytometric analysis of microglia isolated from P0 *dicer$^{fl/fl}$* and newborn *cx3cr1^{Cre}:dicer$^{fl/fl}$* mice revealed decreased proliferation rate in mutant microglia. Data are expressed as mean ± SEM and statistically analyzed with Student's T test (**P<0.01); *dicer$^{fl/fl}$* (n=6), *cx3cr1^{Cre}:dicer$^{fl/fl}$* (n=4).

Figure 7. Prenatal Dicer ablation causes accumulation of DNA damage and renders microglia radio-sensitive

(A) Representative image of comet analysis (left) and a graphical summary (right) of DNA distribution between head and tail of sorted newborn microglia isolated from *cx3cr1^{Cre}:dicer$^{fl/fl}$* and *dicer$^{fl/fl}$* mice. Data are expressed as mean ± SEM and statistically analyzed with Student's T test (*P<0.05, ****P<0.0001). n=3 per group.
(B) Representative picture of FACS analysis (left) and a graphical summary (right) of the frequencies for early and late apoptotic microglia of *cx3cr1^{Cre}:dicer$^{fl/fl}$* and *dicer$^{fl/fl}$*

adult mice, which were analyzed untreated or 24hr after irradiation. Data are expressed as mean ± SEM and statistically analyzed with Student's T test (*P<0.05, ***P<0.001); n=3 per group.

(C) Representative FACS analysis of brains of [*cx3cr1*$^{gfp/+}$ (*CD45.1)* > *dicer*$^{fl/fl}$] and [*cx3cr1*$^{gfp/+}$ (*CD45.1)* > *cx3cr1*^{Cre}*:dicer*$^{fl/fl}$] BM chimeras, 6 weeks after transplantation.

(D) Graphical summary of FACS analysis of chimeric mice, including [*cx3cr1*$^{gfp/+}$ (*CD45.1)* > *dicer*$^{fl/fl}$] and [*cx3cr1*$^{gfp/+}$ (*CD45.1)* > *cx3cr1*^{Cre}*:dicer*$^{fl/fl}$] BM chimeras, performed on either adult or newborn (P0) recipients, 6 weeks after transplantation. Replicate number: [*cx3cr1*$^{gfp/+}$ (*CD45.1)* > *dicer*$^{fl/fl}$] (n=6), [*cx3cr1*$^{gfp/+}$ (*CD45.1)* > *cx3cr1*^{Cre}*:dicer*$^{fl/fl}$] (n=5).

REFERENCES

Amit, I., Winter, D.R., and Jung, S. (2016). The role of the local environment and epigenetics in shaping macrophage identity and their effect on tissue homeostasis. Nat Immunol *17*, 18–25.

Banerjee, S., Xie, N., Cui, H., Tan, Z., Yang, S., Icyuz, M., Abraham, E., and Liu, G. (2013). MicroRNA let-7c Regulates Macrophage Polarization. J. Immunol. *190*, 6542–6549.

Bartel, D.P. (2009). MicroRNAs: target recognition and regulatory functions. Cell *136*, 215–233.

Bernstein, E., Kim, S.Y., Carmell, M.A., Murchison, E.P., Alcorn, H., Li, M.Z., Mills, A.A., Elledge, S.J., Anderson, K.V., and Hannon, G.J. (2003). Dicer is essential for mouse development. Nat Genet *35*, 215–217.

Bertrand, J.Y., Jalil, A., Klaine, M., Jung, S., Cumano, A., and Godin, I. (2005). Three pathways to mature macrophages in the early mouse yolk sac. Blood *106*, 3004–3011.

Bruttger, J., Karram, K., Wörtge, S., Regen, T., Marini, F., Hoppmann, N., Klein, M., Blank, T., Yona, S., Wolf, Y., et al. (2015). Genetic Cell Ablation Reveals Clusters of Local Self-Renewing Microglia in the Mammalian Central Nervous System. Immunity *43*, 92–106.

Butovsky, O., Jedrychowski, M.P., Moore, C.S., Cialic, R., Lanser, A.J., Gabriely, G., Koeglsperger, T., Dake, B., Wu, P.M., Doykan, C.E., et al. (2014). Identification of a unique TGF-β-dependent molecular and functional signature in microglia. Nat Neurosci *17*, 131–143.

Butovsky, O., Siddiqui, S., Gabriely, G., Lanser, A.J., Dake, B., Murugaiyan, G., Doykan, C.E., Wu, P.M., Gali, R.R., Iyer, L.K., et al. (2012). Modulating inflammatory monocytes with a unique microRNA gene signature ameliorates murine ALS. J. Clin. Invest. *122*, 3063–3087.

Buttgereit, A., Lelios, I., Yu, X., Vrohlings, M., Krakoski, N.R., Gautier, E.L., Nishinakamura, R., Becher, B., and Greter, M. (2016). Sall1 is a transcriptional regulator defining microglia identity and function. Nat Immunol.

Cellier, M.F., Courville, P., and Campion, C. (2007). Nramp1 phagocyte intracellular metal withdrawal defense. Microbes Infect. *9*, 1662–1670.

Cheloufi, S., Santos, Dos, C.O., Chong, M.M.W., and Hannon, G.J. (2010). A dicer-independent miRNA biogenesis pathway that requires Ago catalysis. Nature *465*, 584–589.

Chen, J., Buchanan, J.B., Sparkman, N.L., Godbout, J.P., Freund, G.G., and Johnson, R.W. (2008). Neuroinflammation and disruption in working memory in aged mice after acute stimulation of the peripheral innate immune system. Brain, Behavior, and Immunity *22*, 301–311.

Davalos, D., Grutzendler, J., Yang, G., Kim, J.V., Zuo, Y., Jung, S., Littman, D.R., Dustin, M.L., and Gan, W.-B. (2005). ATP mediates rapid microglial response to local brain injury in vivo. Nat Neurosci *8*, 752–758.

Dennis, G., Sherman, B.T., Hosack, D.A., Yang, J., Gao, W., Lane, H.C., and Lempicki, R.A. (2003). DAVID: Database for Annotation, Visualization, and Integrated Discovery. Genome Biol *4*, P3.

Francia, S., Michelini, F., Saxena, A., Tang, D., de Hoon, M., Anelli, V., Mione, M., Carninci, P., and d'Adda di Fagagna, F. (2012). Site-specific DICER and DROSHA RNA products control the DNA-damage response. Nature *488*, 231–235.

Fuhrmann, M., Bittner, T., Jung, C.K.E., Burgold, S., Page, R.M., Mitteregger, G., Haass, C., LaFerla, F.M., Kretzschmar, H., and Herms, J. (2010). Microglial Cx3cr1 knockout prevents neuron loss in a mouse model of Alzheimer's disease. Nature Publishing Group *13*, 411–413.

Gelfand, B.D., Wright, C.B., Kim, Y., Yasuma, T., Yasuma, R., Li, S., Fowler, B.J., Bastos-Carvalho, A., Kerur, N., Uittenbogaard, A., et al. (2015). Iron Toxicity in the Retina Requires Alu RNA and the NLRP3 Inflammasome. CellReports *11*, 1686–1693.

Ginhoux, F., Greter, M., Leboeuf, M., Nandi, S., See, P., Gokhan, S., Mehler, M.F., Conway, S.J., Ng, L.G., Stanley, E.R., et al. (2010). Supporting Fate mapping analysis reveals that adult microglia derive from primitive macrophages. Science *330*, 841–845.

Goldmann, T., Wieghofer, P., Jordao, M.J.C., Prutek, F., Hagemeyer, N., Frenzel, K., Amann, L., Staszewski, O., Kierdorf, K., Krueger, M., et al. (2016). Origin, fate and dynamics of macrophages at central nervous system interfaces. Nat Immunol *17*, 797–805.

Goldmann, T., Wieghofer, P., ller, P.F.M.U., Wolf, Y., Varol, D., Yona, S., Brendecke, S.M., Kierdorf, K., Staszewski, O., Datta, M., et al. (2013). A new type of microglia gene targeting shows TAK1 to be pivotal in CNS autoimmune inflammation. Nature Publishing Group *16*, 1618–1626.

Gosselin, D., Link, V.M., Romanoski, C.E., Fonseca, G.J., Eichenfield, D.Z., Spann, N.J., Stender, J.D., Chun, H.B., Garner, H., Geissmann, F., et al. (2014). Environment Drives Selection and Function of Enhancers Controlling Tissue-Specific Macrophage Identities. Cell *159*, 1327–1340.

Guerreiro, R., and Hardy, J. (2013). TREM2 and neurodegenerative disease. N. Engl. J. Med. *369*, 1569–1570.

Guo, H., Ingolia, N.T., Weissman, J.S., and Bartel, D.P. (2010). Mammalian microRNAs predominantly act to decrease target mRNA levels. Nature *466*, 835–840.

Habbas, S., Santello, M., Becker, D., Stubbe, H., Zappia, G., Liaudet, N., Klaus, F.R., Kollias, G., Fontana, A., Pryce, C.R., et al. (2015). Neuroinflammatory TNFα Impairs Memory via Astrocyte Signaling. Cell *163*, 1730–1741.

Harfe, B.D., McManus, M.T., Mansfield, J.H., Hornstein, E., and Tabin, C.J. (2005). The RNaseIII enzyme Dicer is required for morphogenesis but not patterning of the vertebrate limb. Proc. Natl. Acad. Sci. U.S.a. *102*, 10898–10903.

Harry, G.J. (2013). Microglia during development and aging. Pharmacology and Therapeutics *139*, 313–326.

Heinz, S., Benner, C., Spann, N., Bertolino, E., Lin, Y.C., Laslo, P., Cheng, J.X., Murre, C., Singh, H., and Glass, C.K. (2010). Simple Combinations of Lineage-Determining Transcription Factors Prime cis-Regulatory Elements Required for Macrophage and B Cell Identities. Molecular Cell *38*, 576–589.

Iliopoulos, D., Hirsch, H.A., and Struhl, K. (2009). An Epigenetic Switch Involving NF-κB, Lin28, Let-7 MicroRNA, and IL6 Links Inflammation to Cell Transformation. Cell

139, 693–706.

Jaitin, D.A., Kenigsberg, E., Keren-Shaul, H., Elefant, N., Paul, F., Zaretsky, I., Mildner, A., Cohen, N., Jung, S., Tanay, A., et al. (2014). Massively parallel single-cell RNA-seq for marker-free decomposition of tissues into cell types. Science *343*, 776–779.

Jung, S., Aliberti, J., Graemmel, P., Sunshine, M.J., Kreutzberg, G.W., Sher, A., and Littman, D.R. (2000). Analysis of fractalkine receptor CX(3)CR1 function by targeted deletion and green fluorescent protein reporter gene insertion. Molecular and Cellular Biology *20*, 4106–4114.

Kaneko, H., Dridi, S., Tarallo, V., Gelfand, B.D., Fowler, B.J., Cho, W.G., Kleinman, M.E., Ponicsan, S.L., Hauswirth, W.W., Chiodo, V.A., et al. (2011). DICER1 deficit induces Alu RNA toxicity in age-related macular degeneration. Nature *471*, 325–330.

Kierdorf, K., Erny, D., Goldmann, T., Sander, V., Schulz, C., Perdiguero, E.G., Wieghofer, P., Heinrich, A., Riemke, P., Hölscher, C., et al. (2013). Microglia emerge from erythromyeloid precursors via Pu.1- and Irf8-dependent pathways. Nat Neurosci.

Kiermayer, C., Conrad, M., Schneider, M., Schmidt, J., and Brielmeier, M. (2007). Optimization of spatiotemporal gene inactivation in mouse heart by oral application of tamoxifen citrate. Genesis *45*, 11–16.

Kim, V.N., Han, J., and Siomi, M.C. (2009). Biogenesis of small RNAs in animals. Nat Rev Mol Cell Biol *10*, 126–139.

Kohman, R.A., and Rhodes, J.S. (2013). Neurogenesis, inflammation and behavior. Brain, Behavior, and Immunity *27*, 22–32.

Koralov, S.B., Muljo, S.A., Galler, G.R., Krek, A., Chakraborty, T., Kanellopoulou, C., Jensen, K., Cobb, B.S., Merkenschlager, M., Rajewsky, N., et al. (2008). Dicer Ablation Affects Antibody Diversity and Cell Survival in the B Lymphocyte Lineage. Cell *132*, 860–874.

Kuipers, H., Schnorfeil, F.M., Fehling, H.J., Bartels, H., and Brocker, T. (2010). Dicer-Dependent MicroRNAs Control Maturation, Function, and Maintenance of Langerhans Cells In Vivo. J. Immunol. *185*, 400–409.

Lawson, L.J., Perry, V.H., and Gordon, S. (1992). Turnover of resident microglia in the normal adult mouse brain. Neuroscience *48*, 405–415.

Maggio, N., and Segal, M. (2007). Striking variations in corticosteroid modulation of long-term potentiation along the septotemporal axis of the hippocampus. J. Neurosci. *27*, 5757–5765.

Maggio, N., Shavit-Stein, E., Dori, A., Blatt, I., and Chapman, J. (2013). Prolonged systemic inflammation persistently modifies synaptic plasticity in the hippocampus: modulation by the stress hormones. Front Mol Neurosci *6*, 46.

Mancino, A., Habbeddine, M., Johnson, E., Luron, L., Bebien, M., Memet, S., Fong, C., Bajénoff, M., Wu, X., Karin, M., et al. (2013). I kappa B kinase alpha (IKKα) activity is required for functional maturation of dendritic cells and acquired immunity to infection. Embo J *32*, 816–828.

Mass, E., Ballesteros, I., Farlik, M., Halbritter, F., Günther, P., Crozet, L., Jacome-Galarza, C.E., Händler, K., Klughammer, J., Kobayashi, Y., et al. (2016). Specification of tissue-

resident macrophages during organogenesis. Science 1–22.

Matcovitch-Natan, O., Winter, D.R., Giladi, A., Vargas Aguilar, S., Spinrad, A., Sarrazin, S., Ben-Yehuda, H., David, E., Zelada González, F., Perrin, P., et al. (2016). Microglia development follows a stepwise program to regulate brain homeostasis. Science aad8670.

McKinnon, P.J. (2013). Maintaining genome stability in the nervous system. Nat Neurosci *16*, 1523–1529.

Mildner, A., Schmidt, H., Nitsche, M., Merkler, D., Hanisch, U.-K., Mack, M., Heikenwalder, M., Brück, W., Priller, J., and Prinz, M. (2007). Microglia in the adult brain arise from Ly-6ChiCCR2+ monocytes only under defined host conditions. Nat Neurosci *10*, 1544–1553.

Nimmerjahn, A., Nimmerjahn, A., Kirchhoff, F., and Helmchen, F. (2005). Resting microglial cells are highly dynamic surveillants of brain parenchyma in vivo. Science *308*, 1314–1318.

O'connell, R.M., Rao, D.S., and Baltimore, D. (2012). microRNA regulation of inflammatory responses. Annu. Rev. Immunol. *30*, 295–312.

Olive, P.L., and Banáth, J.P. (2006). The comet assay: a method to measure DNA damage in individual cells. Nat Protoc *1*, 23–29.

Orłowski, D., Sołtys, Z., and Janeczko, K. (2003). Morphological development of microglia in the postnatal rat brain. International Journal of Developmental Neuroscience *21*, 445–450.

Paolicelli, R.C., Bolasco, G., Pagani, F., Maggi, L., Scianni, M., Panzanelli, P., Maurizio Giustetto, Ferreira, T.A., Guiducci, E., Dumas, L., et al. (2012). Synaptic Pruning by Microglia Is Necessary for Normal Brain Development. 1–3.

Poliani, P.L., Wang, Y., Fontana, E., Robinette, M.L., Yamanishi, Y., Gilfillan, S., and Colonna, M. (2015). TREM2 sustains microglial expansion during aging and response to demyelination. J. Clin. Invest. *125*, 2161–2170.

Prinz, M., and Priller, J. (2014). Microglia and brain macrophages in the molecular age: from origin to neuropsychiatric disease. Nat Rev Neurosci *15*, 300–312.

Rademakers, R., Baker, M., Nicholson, A.M., Rutherford, N.J., Finch, N., Soto-Ortolaza, A., Lash, J., Wider, C., Wojtas, A., DeJesus-Hernandez, M., et al. (2012). Mutations in the colony stimulating factor 1 receptor (CSF1R) gene cause hereditary diffuse leukoencephalopathy with spheroids. Nat Genet *44*, 200–205.

Riazi, K., Galic, M.A., Kentner, A.C., Reid, A.Y., Sharkey, K.A., and Pittman, Q.J. (2015). Microglia-dependent alteration of glutamatergic synaptic transmission and plasticity in the hippocampus during peripheral inflammation. J. Neurosci. *35*, 4942–4952.

Saba, R., Gushue, S., Huzarewich, R.L.C.H., Manguiat, K., Medina, S., Robertson, C., and Booth, S.A. (2012). MicroRNA 146a (miR-146a) Is Over-Expressed during Prion Disease and Modulates the Innate Immune Response and the Microglial Activation State. PLoS ONE *7*, e30832–16.

Schaefer, A., O'Carroll, D., Tan, C.L., Hillman, D., Sugimori, M., Llinas, R., and Greengard, P. (2007). Cerebellar neurodegeneration in the absence of microRNAs. J. Exp. Med. *204*, 1553–1558.

Schafer, D.P., Lehrman, E.K., Kautzman, A.G., Koyama, R., Mardinly, A.R., Yamasaki, R.,

Ransohoff, R.M., Greenberg, M.E., Barres, B.A., and Stevens, B. (2012). Microglia Sculpt Postnatal Neural Circuits in an Activity and Complement-Dependent Manner. Neuron *74*, 691–705.

Schmiedel, J.M., Klemm, S.L., Zheng, Y., Sahay, A., Blüthgen, N., Marks, D.S., and van Oudenaarden, A. (2015). Gene expression. MicroRNA control of protein expression noise. Science *348*, 128–132.

Squarzoni, P., Oller, G., Hoeffel, G., Pont-Lezica, L., Rostaing, P., Low, D., Bessis, A., Ginhoux, F., and Garel, S. (2014). Microglia modulate wiring of the embryonic forebrain. CellReports *8*, 1271–1279.

Srinivas, S., Watanabe, T., Lin, C.S., William, C.M., Tanabe, Y., Jessell, T.M., and Costantini, F. (2001). Cre reporter strains produced by targeted insertion of EYFP and ECFP into the ROSA26 locus. BMC Dev. Biol. *1*, 4.

Strehl, A., Lenz, M., Itsekson-Hayosh, Z., Becker, D., Chapman, J., Deller, T., Maggio, N., and Vlachos, A. (2014). Systemic inflammation is associated with a reduction in Synaptopodin expression in the mouse hippocampus. Experimental Neurology *261*, 230–235.

Subramanian, A., Tamayo, P., Mootha, V.K., Mukherjee, S., Ebert, B.L., Gillette, M.A., Paulovich, A., Pomeroy, S.L., Golub, T.R., Lander, E.S., et al. (2005). Gene set enrichment analysis: a knowledge-based approach for interpreting genome-wide expression profiles. Proc. Natl. Acad. Sci. U.S.a. *102*, 15545–15550.

Swahari, V., Nakamura, A., Baran-Gale, J., Garcia, I., Crowther, A.J., Sons, R., Gershon, T.R., Hammond, S., Sethupathy, P., and Deshmukh, M. (2016). Essential Function of Dicer in Resolving DNA Damage in the Rapidly Dividing Cells of the Developing and Malignant Cerebellum. CellReports *14*, 216–224.

Taganov, K.D., Boldin, M.P., Chang, K.-J., and Baltimore, D. (2006). NF-kappaB-dependent induction of microRNA miR-146, an inhibitor targeted to signaling proteins of innate immune responses. Proc. Natl. Acad. Sci. U.S.a. *103*, 12481–12486.

Tao, J., Wu, H., Lin, Q., Wei, W., Lu, X.H., Cantle, J.P., Ao, Y., Olsen, R.W., Yang, X.W., Mody, I., et al. (2011). Deletion of Astroglial Dicer Causes Non-Cell-Autonomous Neuronal Dysfunction and Degeneration. Journal of Neuroscience *31*, 8306–8319.

Trapnell, C., Pachter, L., and Salzberg, S.L. (2009). TopHat: discovering splice junctions with RNA-Seq. Bioinformatics *25*, 1105–1111.

Turner, M.L., Schnorfeil, F.M., and Brocker, T. (2011). MicroRNAs Regulate Dendritic Cell Differentiation and Function. The Journal of Immunology *187*, 3911–3917.

Varol, C., Mildner, A., and Jung, S. (2015). Macrophages: Development and Tissue Specialization. Annu. Rev. Immunol. *33*, 643–675.

Vereker, E., Campbell, V., Roche, E., McEntee, E., and Lynch, M.A. (2000). Lipopolysaccharide inhibits long term potentiation in the rat dentate gyrus by activating caspase-1. J. Biol. Chem. *275*, 26252–26258.

Wang, Y., Cella, M., Mallinson, K., Ulrich, J.D., Young, K.L., Robinette, M.L., Gilfillan, S., Krishnan, G.M., Sudhakar, S., Zinselmeyer, B.H., et al. (2015). TREM2 lipid sensing sustains the microglial response in an Alzheimer's disease model. Cell *160*, 1061–1071.

Wei, W., Ba, Z., Gao, M., Wu, Y., Ma, Y., Amiard, S., White, C.I., Danielsen, J.M.R., Yang, Y.-G., and Qi, Y. (2012). A Role for Small RNAs in DNA Double-Strand Break Repair. Cell *149*, 101–112.

Yona, S., Kim, K.-W., Wolf, Y., Mildner, A., Varol, D., Breker, M., Strauss-Ayali, D., Viukov, S., Guilliams, M., Misharin, A., et al. (2013). Fate mapping reveals origins and dynamics of monocytes and tissue macrophages under homeostasis. Immunity *38*, 79–91.

Zhang, L., Dong, L.-Y., Li, Y.-J., Hong, Z., and Wei, W.-S. (2012). The microRNA miR-181c controls microglia-mediated neuronal apoptosis by suppressing tumor necrosis factor. Journal of Neuroinflammation *9*, 211–226.

Zhou, B.B., and Elledge, S.J. (2000). The DNA damage response: putting checkpoints in perspective. Nature *408*, 433–439.

Figure 1-7

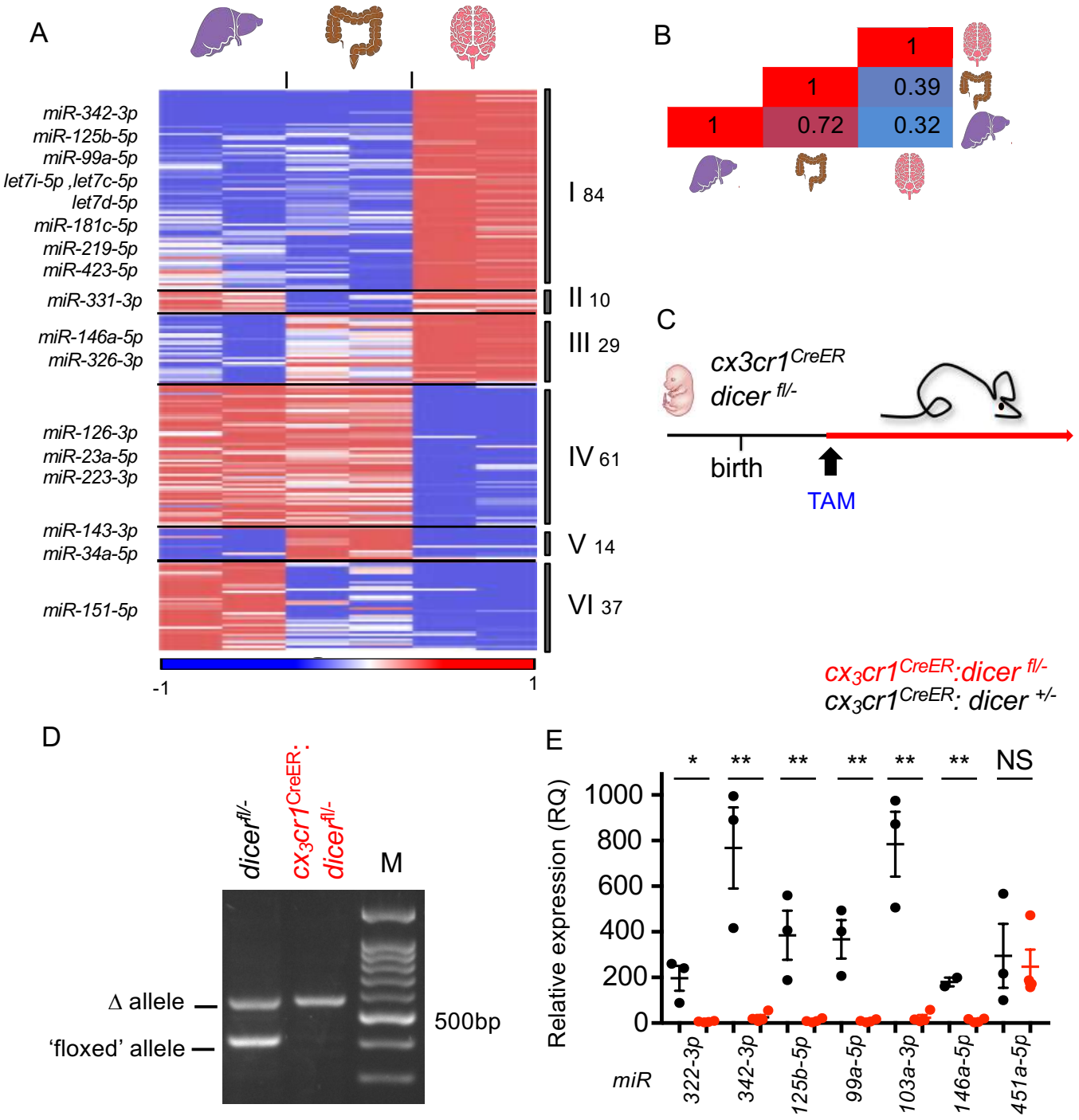

Figure 1

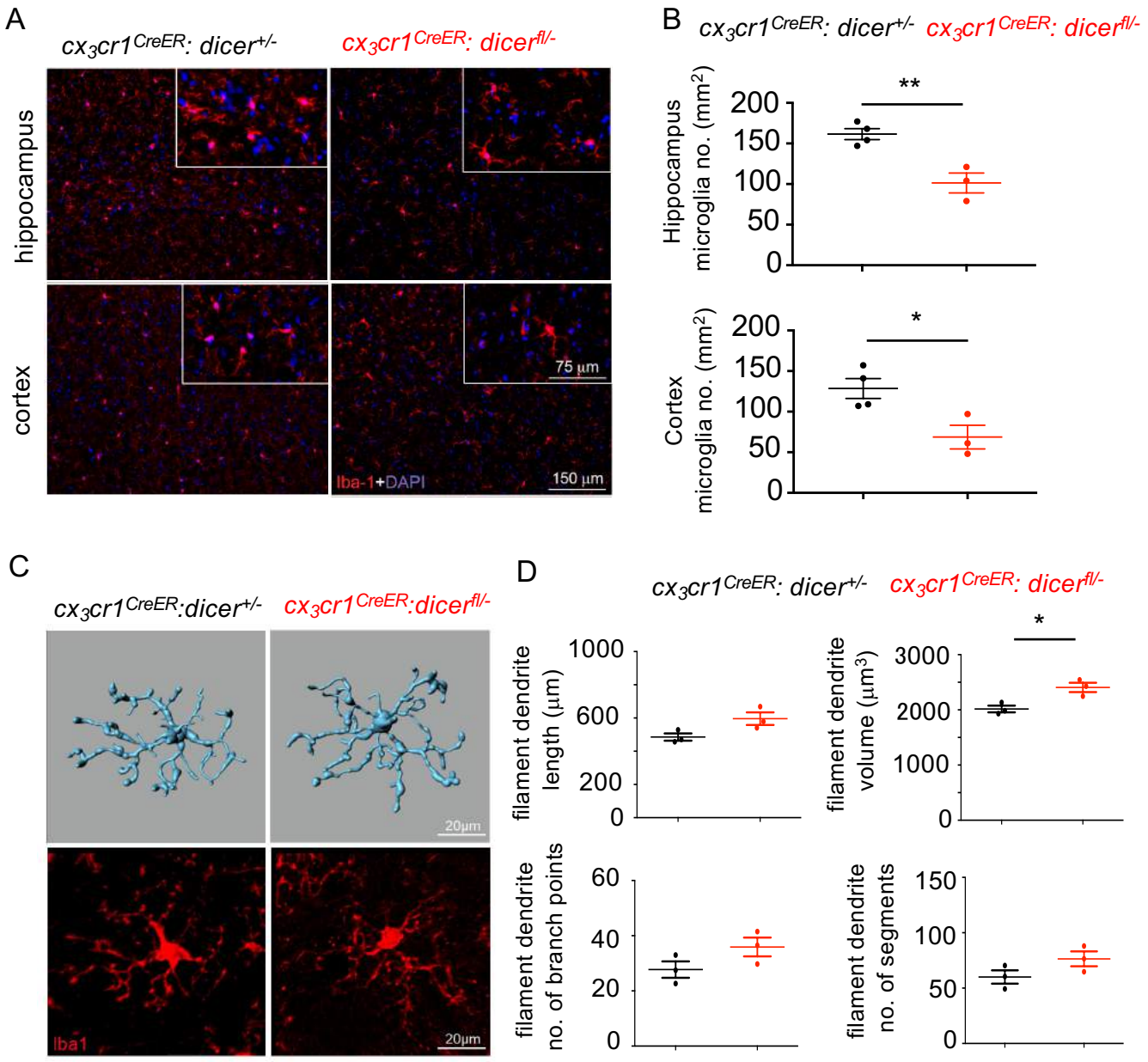
A
cx3cr1CreER: dicer+/-
cx3cr1CreER: dicerfl/-
hippocampus
cortex
75 µm
Iba-1+DAPI
150 µm
B
cx3cr1CreER: dicer+/-
cx3cr1CreER: dicerfl/-
Hippocampus microglia no. (mm2)
**
200
150
100
50
0
Cortex microglia no. (mm2)
*
C
cx3cr1CreER:dicer+/-
cx3cr1CreER:dicerfl/-
20µm
Iba1
D
cx3cr1CreER: dicer+/-
cx3cr1CreER: dicerfl/-
filament dendrite length (µm)
1000
600
200
0
filament dendrite volume (µm3)
*
3000
2000
1000
filament dendrite no. of branch points
60
40
20
filament dendrite no. of segments
150
100
50

Figure 2

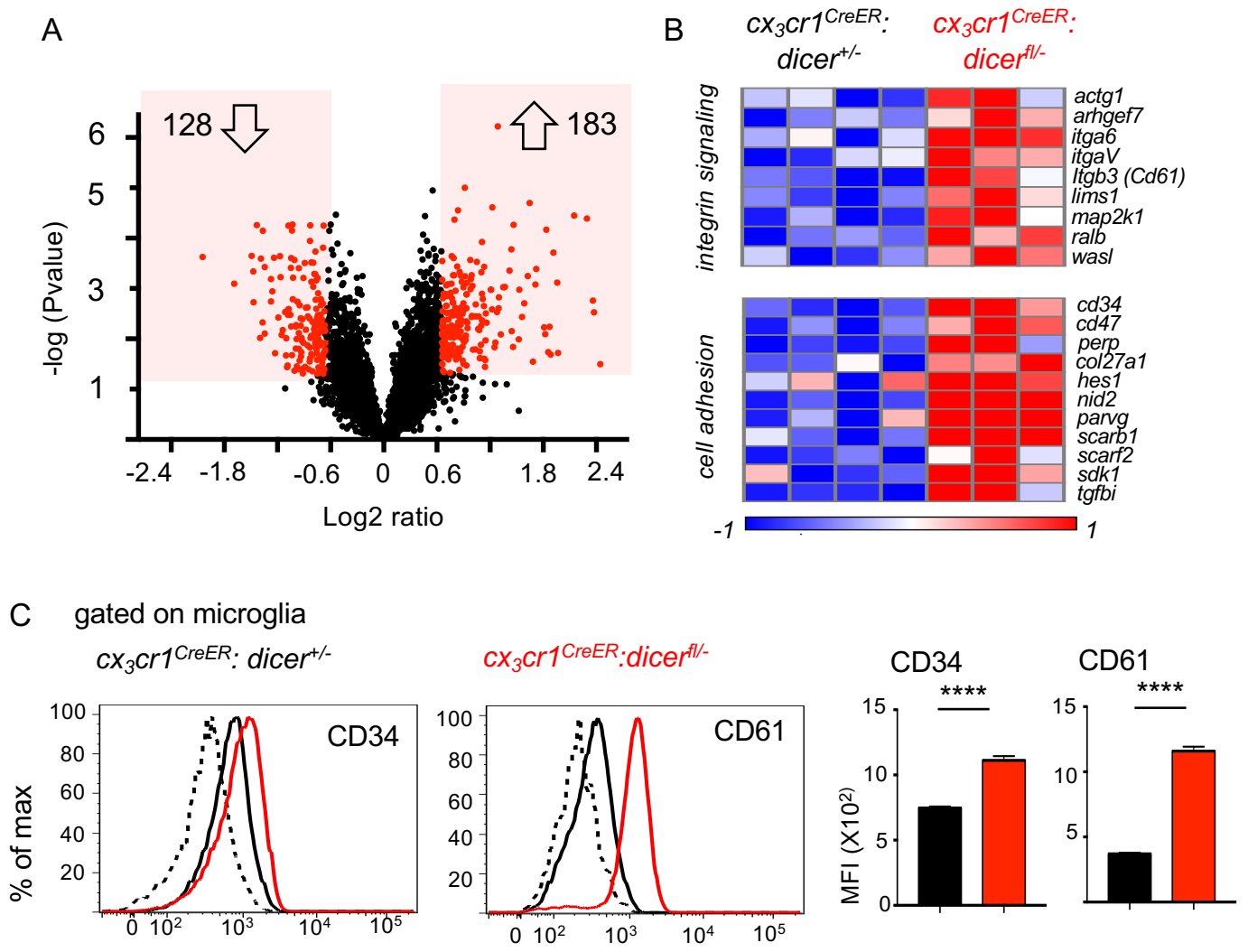
A
128
183
-log (Pvalue)
Log2 ratio
B
cx3cr1CreER: dicer+/-
cx3cr1CreER: dicerfl/-
integrin signaling
cell adhesion
actg1
arhgef7
itga6
itgaV
Itgb3 (Cd61)
lims1
map2k1
ralb
wasl
cd34
cd47
perp
col27a1
hes1
nid2
parvg
scarb1
scarf2
sdk1
tgfbi
-1
1
C
gated on microglia
cx3cr1CreER: dicer+/-
cx3cr1CreER:dicerfl/-
CD34
CD61
% of max
MFI (X10²)
****

Figure 3

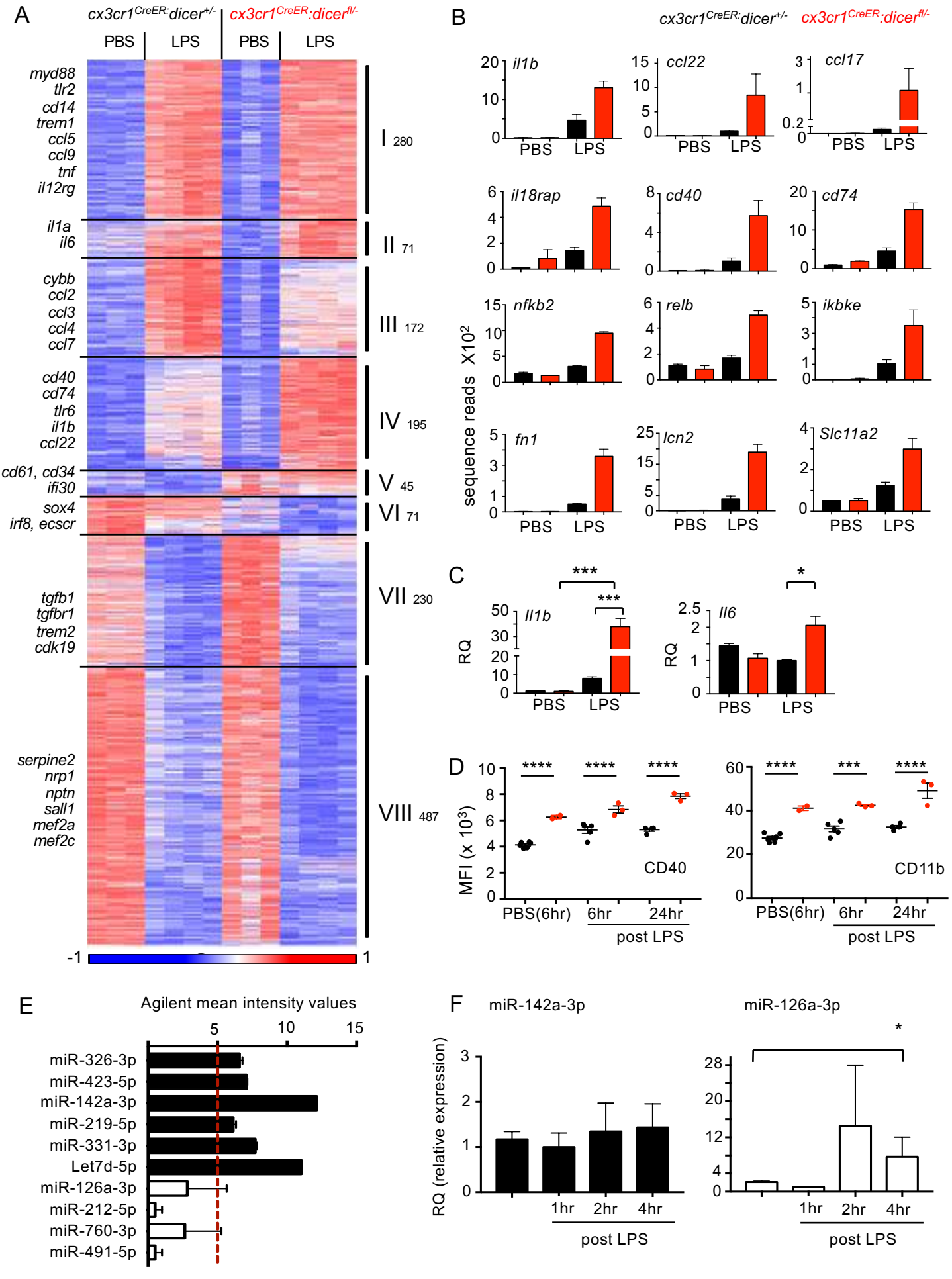
A
cx3cr1CreER:dicer+/-
cx3cr1CreER:dicerfl/-
PBS
LPS
PBS
LPS
myd88
tlr2
cd14
trem1
ccl5
ccl9
tnf
il12rg
I 280
il1a
il6
II 71
cybb
ccl2
ccl3
ccl4
ccl7
III 172
cd40
cd74
tlr6
il1b
ccl22
IV 195
cd61, cd34
ifi30
V 45
sox4
irf8, ecscr
VI 71
tgfb1
tgfbr1
trem2
cdk19
VII 230
serpine2
nrp1
nptn
sall1
mef2a
mef2c
VIII 487
-1
1
B
cx3cr1CreER:dicer+/-
cx3cr1CreER:dicerfl/-
il1b
ccl22
ccl17
il18rap
cd40
cd74
nfkb2
relb
ikbke
fn1
lcn2
Slc11a2
sequence reads X10²
PBS
LPS
C
Il1b
Il6
RQ
***
*
D
MFI (x 10³)
CD40
CD11b
PBS(6hr)
6hr
24hr
post LPS
****
***
E
Agilent mean intensity values
miR-326-3p
miR-423-5p
miR-142a-3p
miR-219-5p
miR-331-3p
Let7d-5p
miR-126a-3p
miR-212-5p
miR-760-3p
miR-491-5p
F
miR-142a-3p
miR-126a-3p
RQ (relative expression)
1hr
2hr
4hr
post LPS

Figure 4

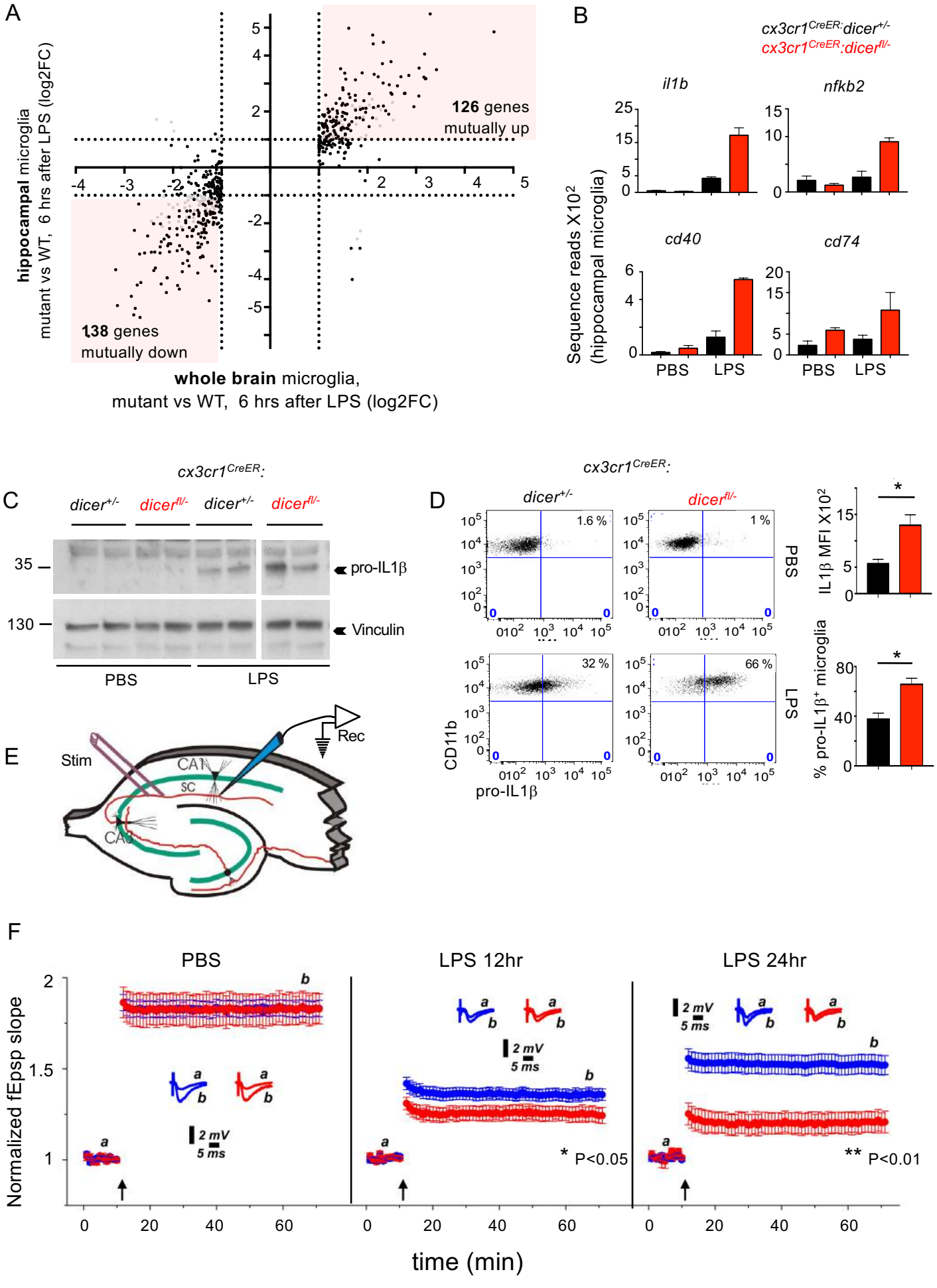
A
hippocampal microglia
mutant vs WT, 6 hrs after LPS (log2FC)
126 genes
mutually up
138 genes
mutually down
whole brain microglia,
mutant vs WT, 6 hrs after LPS (log2FC)
B
cx3cr1CreER:dicer+/-
cx3cr1CreER:dicerfl/-
il1b
nfkb2
cd40
cd74
Sequence reads X10²
(hippocampal microglia)
PBS
LPS
C
cx3cr1CreER:
dicer+/-
dicerfl/-
35
130
pro-IL1β
Vinculin
PBS
LPS
D
cx3cr1CreER:
1.6 %
1 %
32 %
66 %
CD11b
pro-IL1β
PBS
LPS
IL1β MFI X10²
% pro-IL1β+ microglia
E
Stim
Rec
CA1
SC
CA3
F
PBS
LPS 12hr
LPS 24hr
Normalized fEpsp slope
2 mV
5 ms
* P<0.05
** P<0.01
time (min)

Figure 5

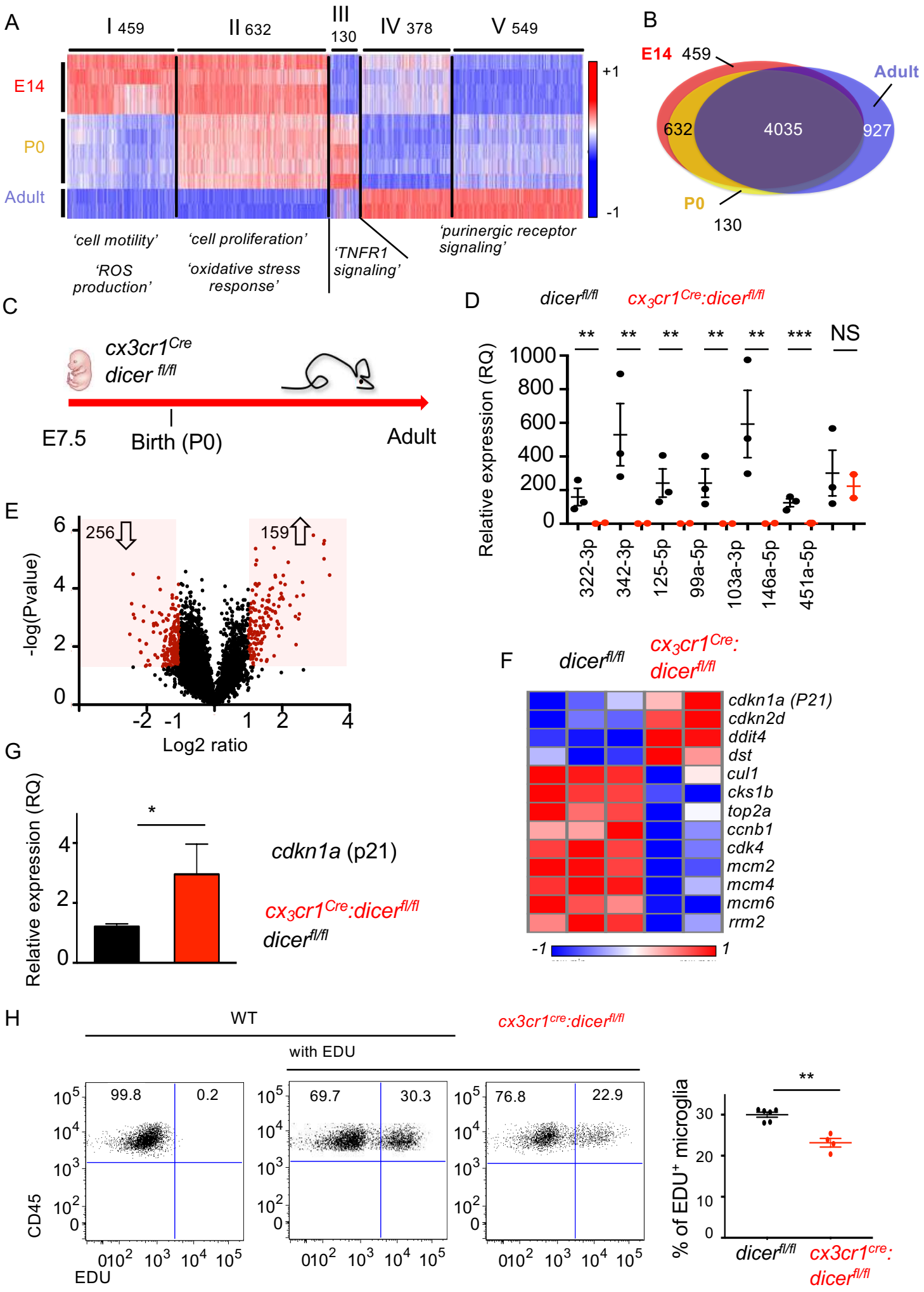
A
I 459
II 632
III 130
IV 378
V 549
E14
P0
Adult
+1
-1
'cell motility'
'ROS production'
'cell proliferation'
'oxidative stress response'
'TNFR1 signaling'
'purinergic receptor signaling'
B
E14 459
Adult
632
4035
927
P0
130
C
cx3cr1Cre
dicer fl/fl
E7.5
Birth (P0)
Adult
D
dicerfl/fl
cx3cr1Cre:dicerfl/fl
Relative expression (RQ)
1000
800
600
400
200
0
** ** ** ** ** *** NS
322-3p
342-3p
125-5p
99a-5p
103a-3p
146a-5p
451a-5p
E
-log(Pvalue)
6
4
2
0
256
159
-2 -1 1 2 4
Log2 ratio
F
dicerfl/fl
cx3cr1Cre:
dicerfl/fl
cdkn1a (P21)
cdkn2d
ddit4
dst
cul1
cks1b
top2a
ccnb1
cdk4
mcm2
mcm4
mcm6
rrm2
-1
1
G
Relative expression (RQ)
4
2
0
*
cdkn1a (p21)
cx3cr1Cre:dicerfl/fl
dicerfl/fl
H
WT
cx3cr1cre:dicerfl/fl
with EDU
CD45
EDU
99.8
0.2
69.7
30.3
76.8
22.9
% of EDU+ microglia
30
20
10
0
**
dicerfl/fl
cx3cr1cre:
dicerfl/fl

Figure 6

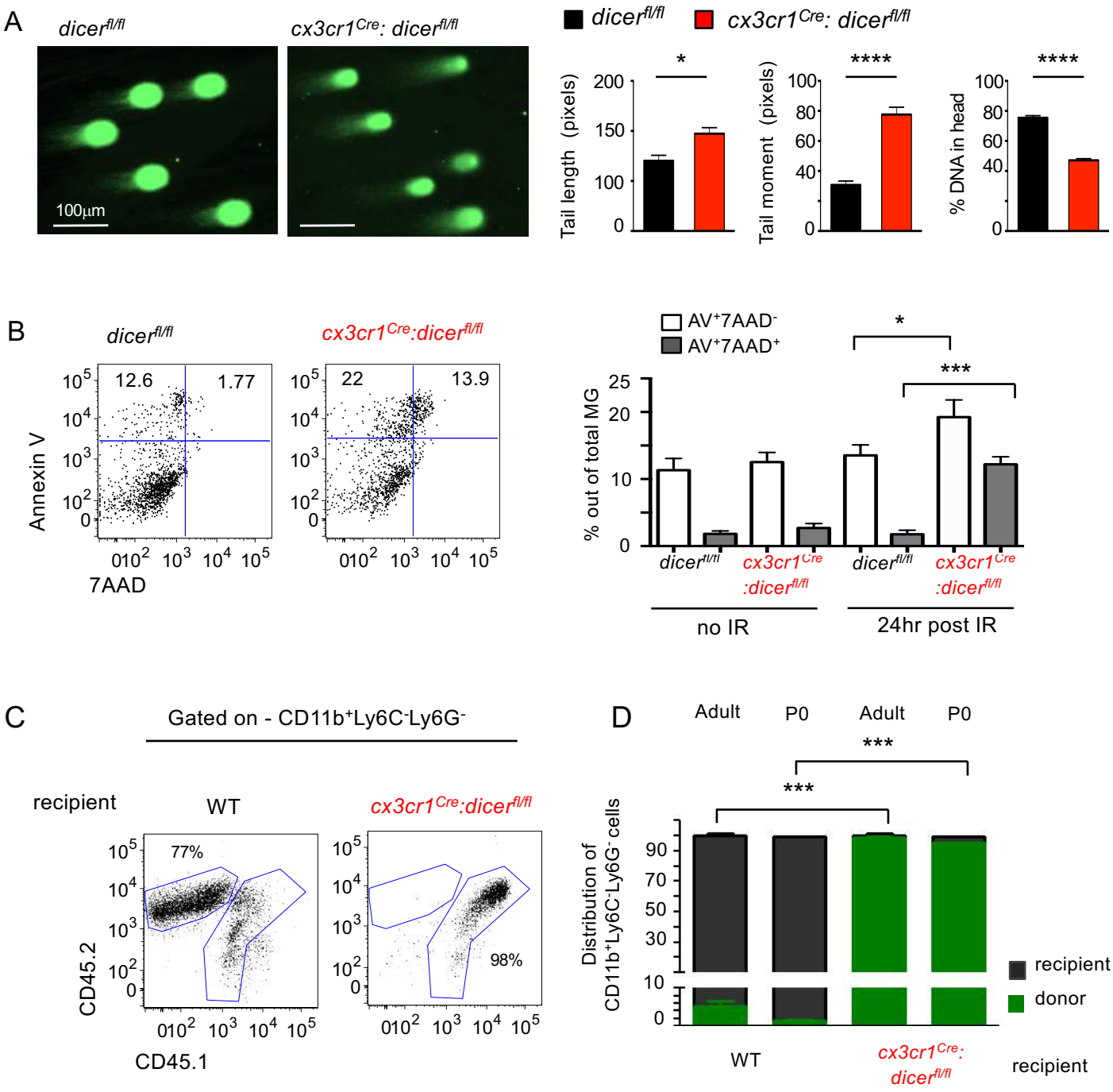
A
dicer fl/fl
cx3cr1 Cre: dicer fl/fl
100µm
dicer fl/fl
cx3cr1 Cre: dicer fl/fl
Tail length (pixels)
Tail moment (pixels)
% DNA in head
*
****
****
B
dicer fl/fl
cx3cr1 Cre :dicer fl/fl
Annexin V
7AAD
12.6
1.77
22
13.9
AV+7AAD-
AV+7AAD+
% out of total MG
*
***
no IR
24hr post IR
C
Gated on - CD11b+Ly6C-Ly6G-
recipient
WT
cx3cr1 Cre :dicer fl/fl
77%
98%
CD45.2
CD45.1
D
Adult
P0
Adult
P0
***
***
Distribution of CD11b+Ly6C-Ly6G- cells
recipient
donor
WT
cx3cr1 Cre : dicer fl/fl
recipient

Figure 7

Click here to download Supplemental Text & Figures Varol et al 2nd revision Suppl Fig 1-9 final .pdf

A

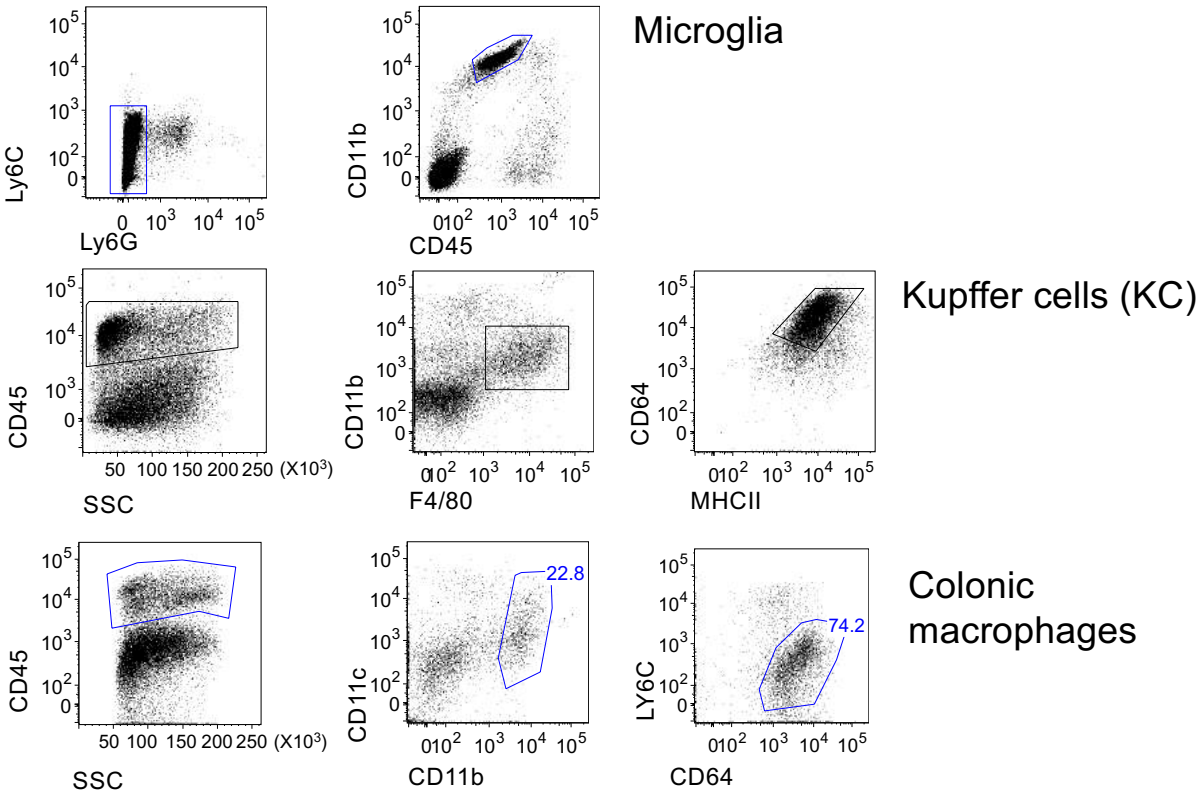

B miRNAs enriched in microglia – cluster 1 (sorted by normalized intensity)

miR i.d	Average normalized intensity	miR i.d	Average normalized intensity	miR i.d	Average normalized intensity	miR i.d	Average normalized intensity
mmu-miR-3963	15.52	mmu-miR-20b-5p	9.155	mmu-miR-455-5p	6.6	mmu-miR-744-5p	5.085
mmu-miR-5100	14.1	mmu-miR-1839-3p	9.075	mmu-miR-301a-3p	6.695	mmu-miR-664-3p	4.995
mmu-miR-15a-5p	13.72	mmu-miR-140-3p	8.74	mmu-miR-342-5p	6.54	mmu-miR-466b-3p	4.86
mmu-miR-29a-3p	13.25	mmu-miR-25-3p	8.81	mmu-miR-148b-3p	6.245	mmu-miR-503-5p	4.75
mmu-miR-16-5p	12.7	mmu-miR-93-5p	8.71	mmu-miR-30e-3p	6.09	mmu-miR-3070a-3p	5.495
mmu-miR-342-3p	12.71	mmu-miR-140-5p	8.365	mmu-miR-219-5p	6.105	mmu-miR-7a-1-3p	4.58
mmu-let-7i-5p	11.915	mmu-miR-425-5p	8.255	mmu-miR-186-5p	5.9	mmu-miR-467b-5p	4.72
mmu-let-7c-5p	11.475	mmu-miR-181b-5p	8.24	mmu-miR-3068-3p	5.855	mmu-miR-150-3p	5.655
mmu-miR-125b-5p	11.245	mmu-miR-100-5p	8	mmu-miR-328-3p	5.815	mmu-miR-124-3p	4.545
mmu-miR-99a-5p	10.845	mmu-miR-338-3p	7.675	mmu-miR-669f-3p	5.71	mmu-miR-29a-5p	4.345
mmu-miR-103-3p	10.62	mmu-miR-1839-5p	7.65	mmu-miR-5110	6.1	mmu-miR-181d-5p	4.395
mmu-miR-690	10.665	mmu-miR-101b-3p	7.45	mmu-miR-3069-3p	5.76	mmu-miR-9-5p	4.28
mmu-miR-92a-3p	10.35	mmu-miR-361-5p	7.335	mmu-miR-21a-3p	5.55	mmu-miR-191-3p	4.205
mmu-miR-107-3p	10.36	mmu-miR-6412	7.19	mmu-miR-181a-1-3p	5.55	mmu-miR-1843a-5p	4.145
mmu-miR-5097	10.26	mmu-miR-5117-3p	7.1	mmu-miR-450a-5p	5.345	mmu-miR-9-3p	4.14
mmu-miR-30c-5p	10.19	mmu-miR-423-5p	7.09	mmu-miR-17-5p	5.435	mmu-miR-29b-1-5p	4.25
mmu-miR-181a-5p	10.065	mmu-miR-17-3p	6.965	mmu-miR-190a-5p	5.23	mmu-miR-32-5p	4.205
mmu-miR-322-5p	9.98	mmu-miR-98-5p	7.16	mmu-miR-128-3p	5.165	mmu-miR-542-3p	4.31
mmu-miR-455-3p	9.315	mmu-miR-152-3p	6.955	mmu-miR-3106-5p	6.275	mmu-miR-505-3p	3.905
mmu-miR-5119	9.42	mmu-miR-181c-5p	6.62	mmu-miR-467e-5p	5.055	mmu-let-7d-3p	4.005

C miRNAs shared by microglia, colonic macrophages and KC

miR i.d	Microglia Average normalized intensity	miR i.d	Microglia Average normalized intensity
mmu-miR-6366	16.08	mmu-miR-142-5p	9.225
mmu-let-7f-5p	12.255	mmu-miR-3096b-3p	8.685
mmu-miR-142-3p	12.125	mmu-miR-30d-5p	8.91
mmu-let-7a-5p	11.97	mmu-miR-652-3p	9.55
mmu-miR-146a-5p	11.75	mmu-miR-106b-5p	9.15
mmu-miR-23a-3p	12.31	mmu-miR-1895	8.38
mmu-miR-3968	11.51	mmu-miR-6368	8.79
mmu-miR-24-3p	11.345	mmu-miR-3072-5p	8.685
mmu-let-7g-5p	11.65	mmu-miR-1897-5p	8.09
mmu-miR-709	10.98	mmu-miR-5112	8.38
mmu-miR-26a-5p	11.195	mmu-miR-500-3p	7.98
mmu-let-7d-5p	11	mmu-miR-378d	7.35
mmu-miR-3473b	10.335	mmu-miR-5107-5p	8.14
mmu-miR-22-3p	10.22	mmu-miR-101a-3p	7.67
mmu-let-7b-5p	10.43	mmu-miR-1904	7.75
mmu-miR-26b-5p	10.89	mmu-miR-671-5p	7.935
mmu-miR-30b-5p	9.495	mmu-miR-378b	7.235
mmu-miR-15b-5p	9.46		
mmu-miR-23b-3p	9.475		
mmu-miR-29c-3p	9.86		

Varol et al., Figure S1

A

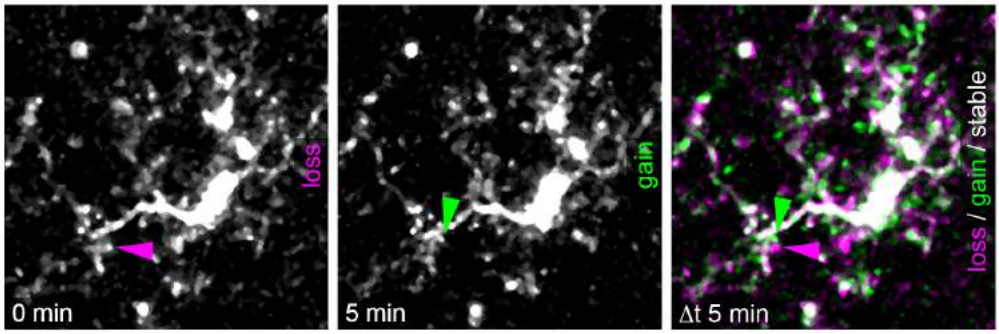

cx3cr1CreER: dicer+/- :r26-YFP *cx3cr1CreER: dicerfl/- :r26-YFP*

B

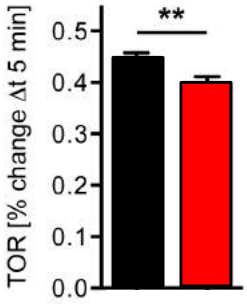

Varol et al., Figure S2

A

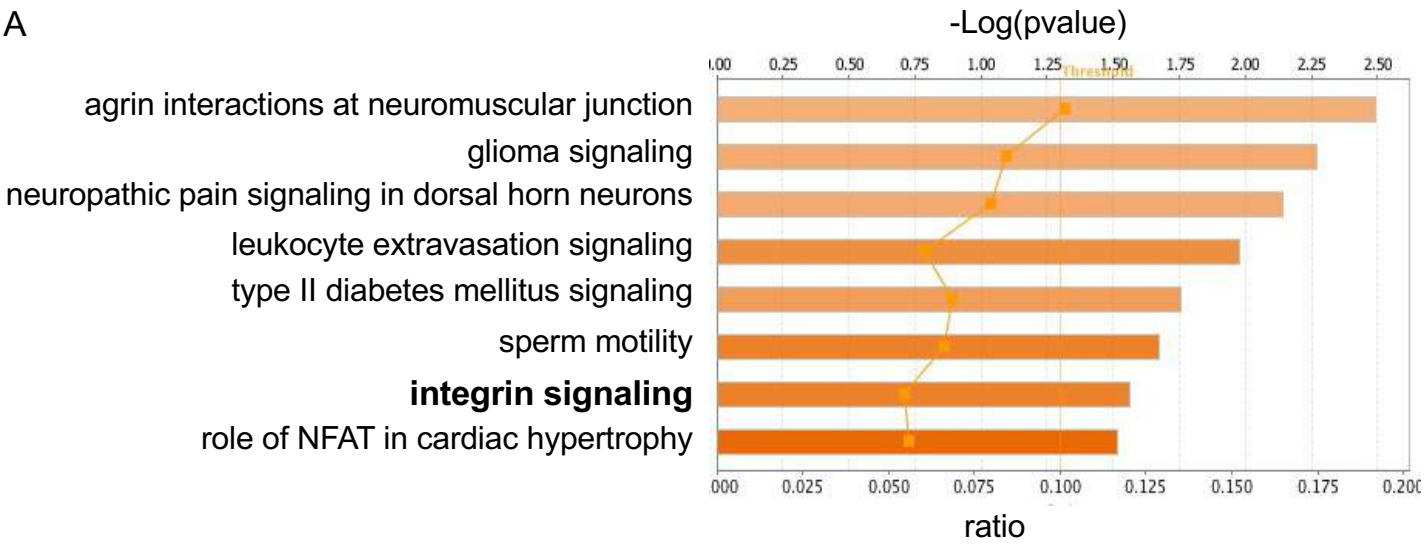

B

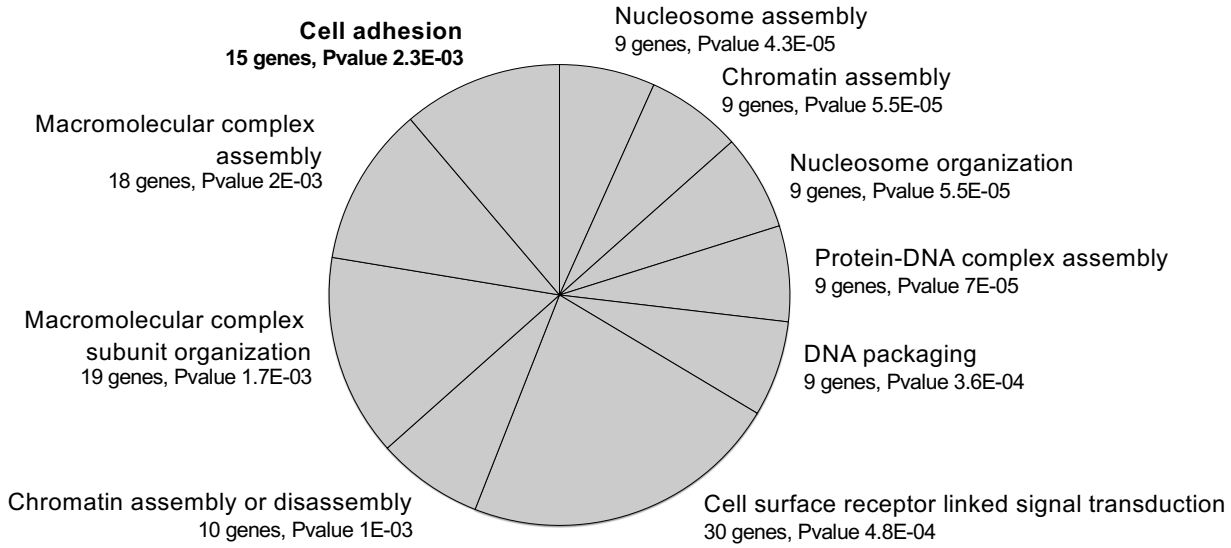

Varol et al., Figure S3

A

Cluster	Go annotation	Benjamini (Pvalue)
I	GO:0002376~immune system process	9.62E-08
I	GO:0009615~response to virus	1.33E-07
I	GO:0051607~defense response to virus	1.11E-06
I	GO:0045071~negative regulation of viral genome replication	4.64E-05
I	GO:0042254~ribosome biogenesis	4.04E-05
I	GO:0045087~innate immune response	3.66E-04
I	GO:0030593~neutrophil chemotaxis	0.00393763
I	GO:0006955~immune response	0.005192394
I	GO:0006364~rRNA processing	0.00502318
IV	GO:0006954~inflammatory response	1.82E-06
IV	GO:0045766~positive regulation of angiogenesis	0.002897105
IV	GO:0071346~cellular response to interferon-gamma	0.012608669
IV	GO:0006955~immune response	0.009768911
IV	GO:0010628~positive regulation of gene expression	0.012597554
IV	GO:0034097~response to cytokine	0.011965022
IV	GO:0030593~neutrophil chemotaxis	0.01094689
IV	GO:0048146~positive regulation of fibroblast proliferation	0.011550116
IV	GO:0002376~immune system process	0.010665648
VII	GO:0030335~positive regulation of cell migration	0.02401279
VIII	GO:0043547~positive regulation of GTPase activity	0.019322938

Varol et al., Figure S4

B

Dicer LPS Vs WT LPS upregulated genes miR signature	Gsea permutation Analysis (Pvalue)	Hyper – geometric (Pvalue)	Expressed in steady state MG (Agilent miR array)
miR-326-3p	0.033	0.000427	*yes*
miR-423-5p	0.016	0.00071	*yes*
miR-142-3p	0	0.00436	*yes*
miR-219-5p	0.04347	0.0438	*yes*
miR-331-3p	0.021	0.0486	*yes*
Let-7d-5p	0	0.05	*yes*
miR-126-3p	0.006	0.0267	*no*
miR-212-5p	0.015	0.0356	*no*
miR-760-3p	0	0.0372	*no*
miR-491-5p	0	0.0443	*no*

C GSEA - histograms

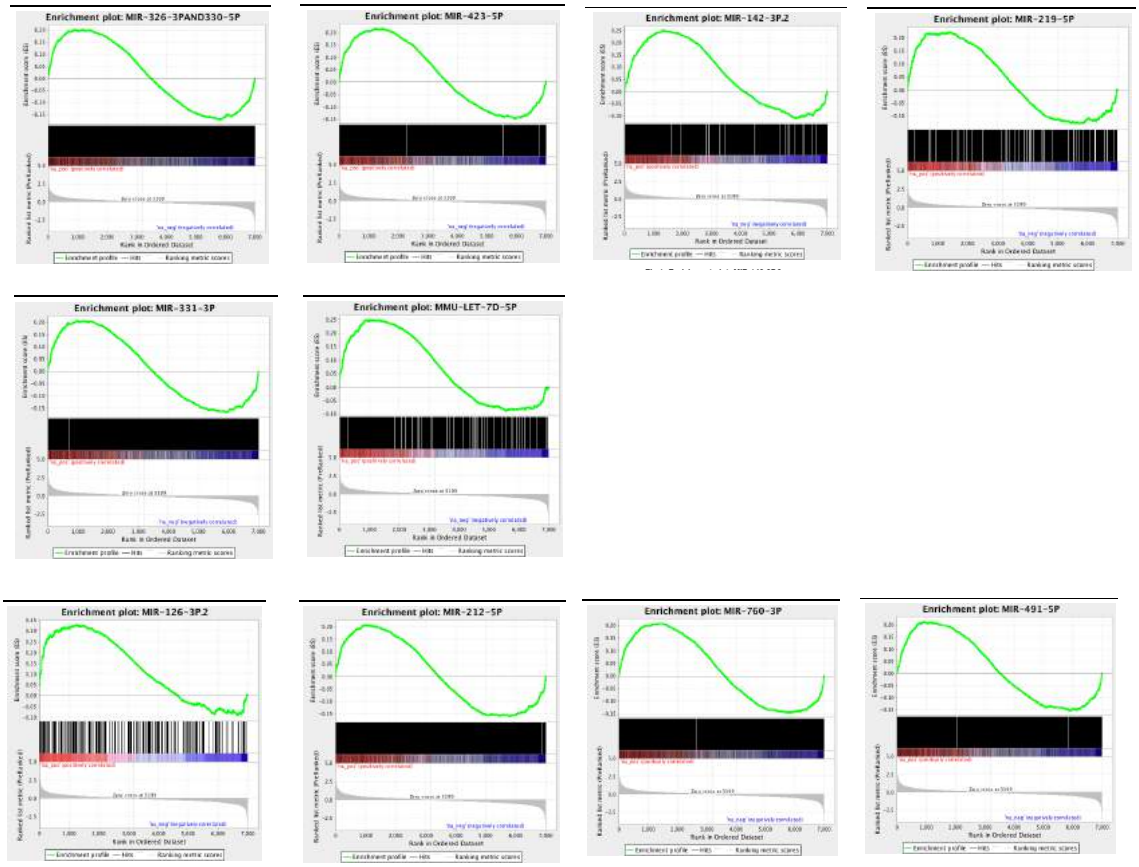

Varol et al., Figure S4

D

cx3cr1$^{CreER:}$*dicer*$^{+/-}$

cx3cr1^{CreER}*:dicer*$^{fl/-}$

LPS challenge

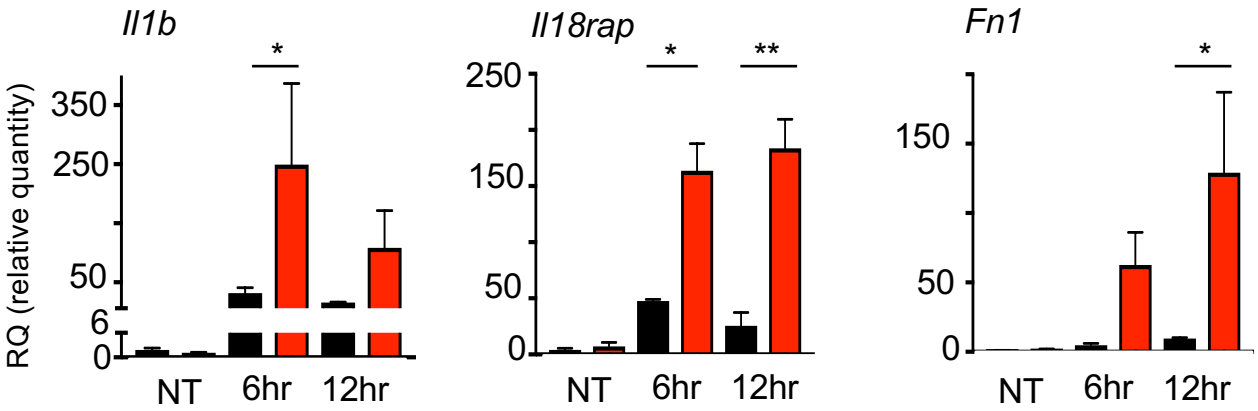

poly I:C challenge

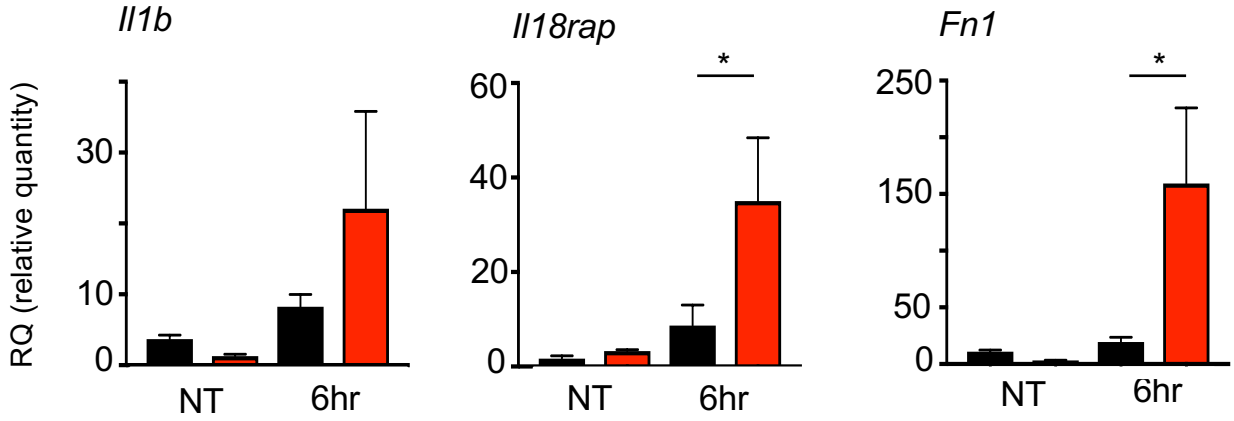

Varol et al., Figure S4

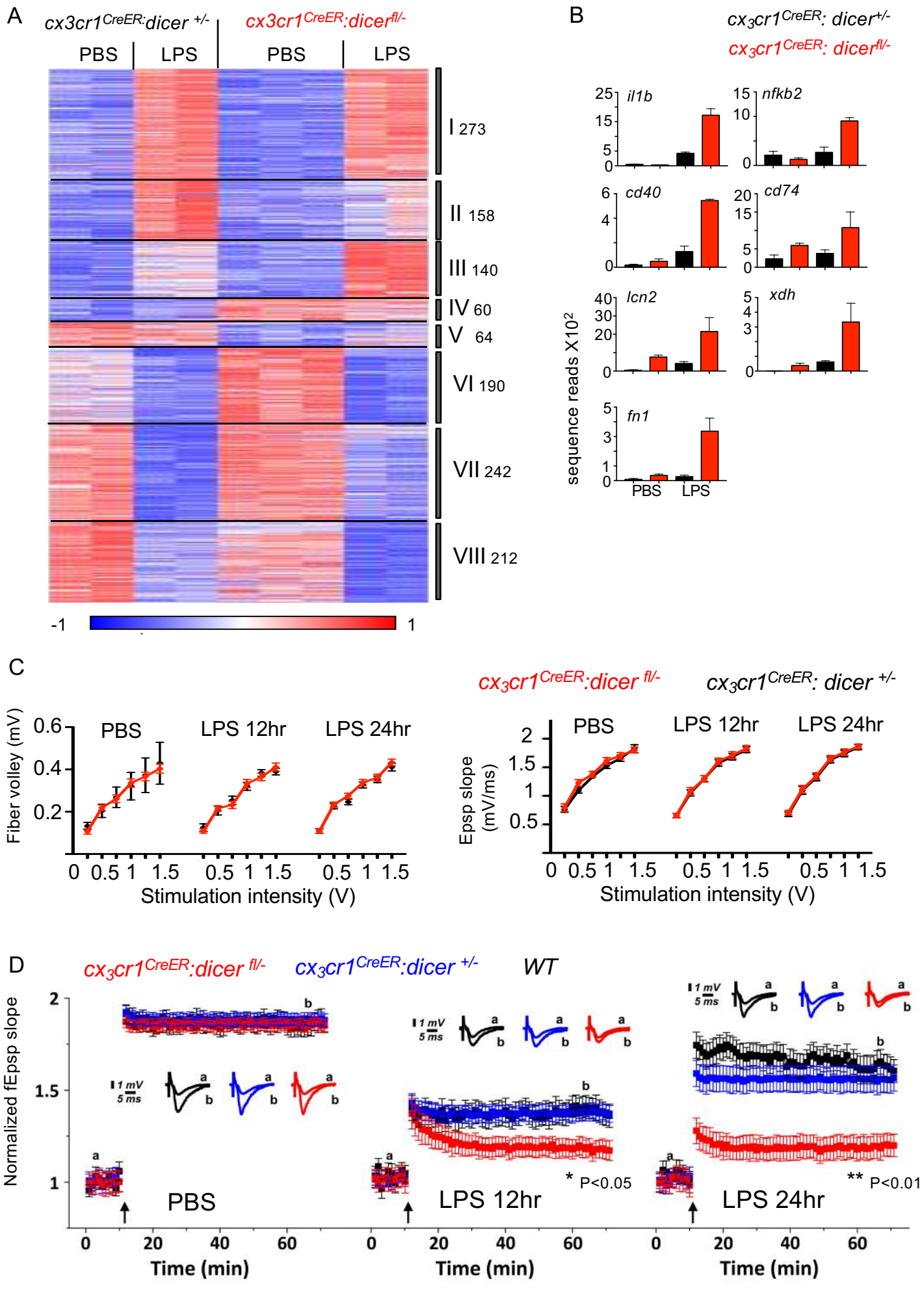

Varol et al., Figure S5

A P0 *cx3cr1*^{Cre}*:dicer*$^{fl/fl}$ *microglia*
Top changed canonical pathways
(Ingenuity pathway analysis)

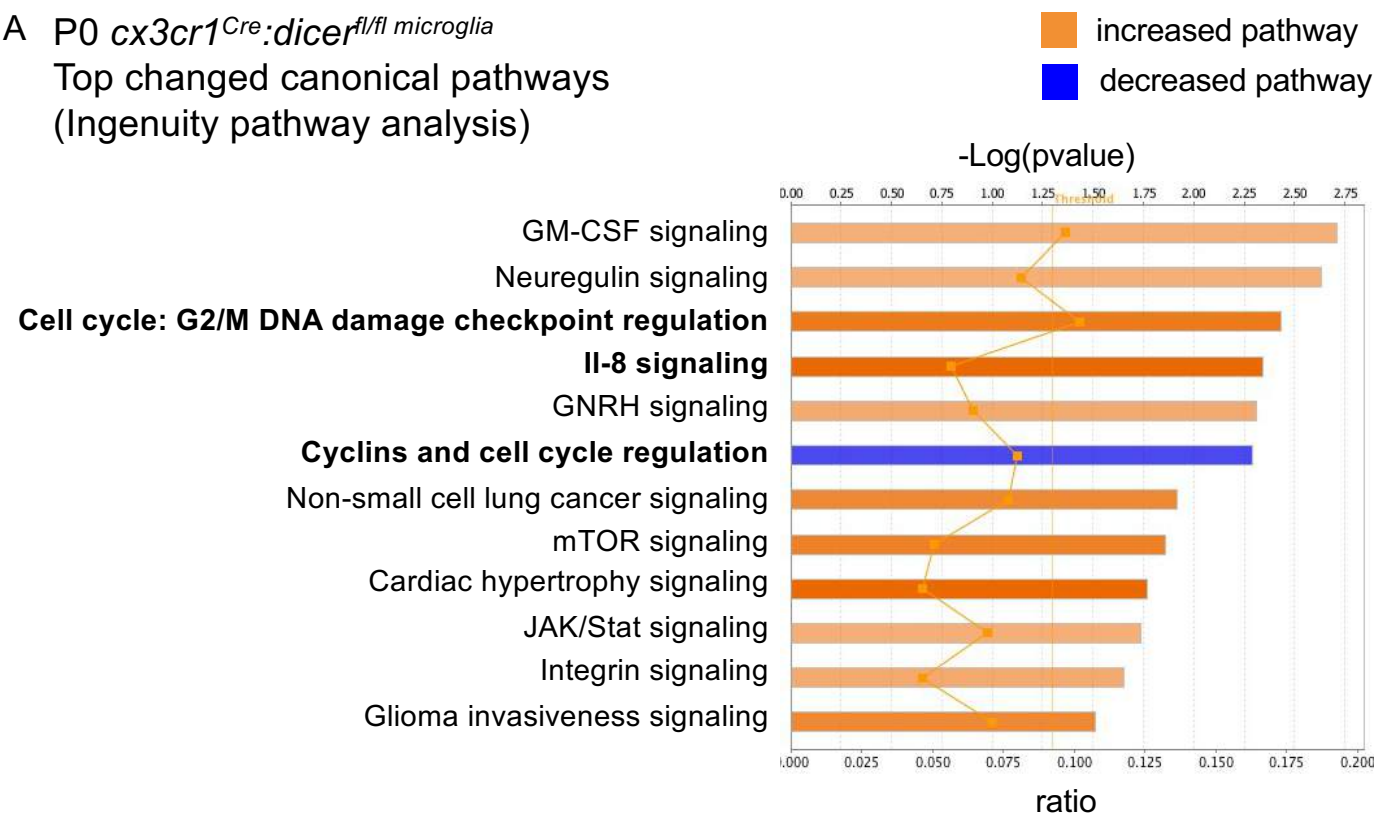

B

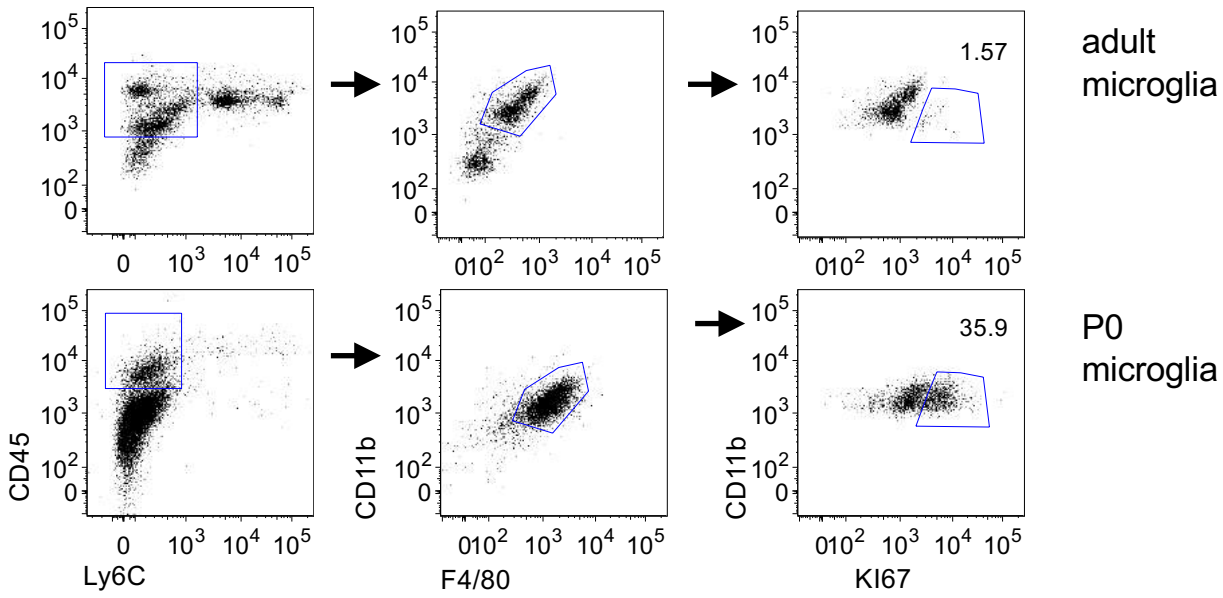

C

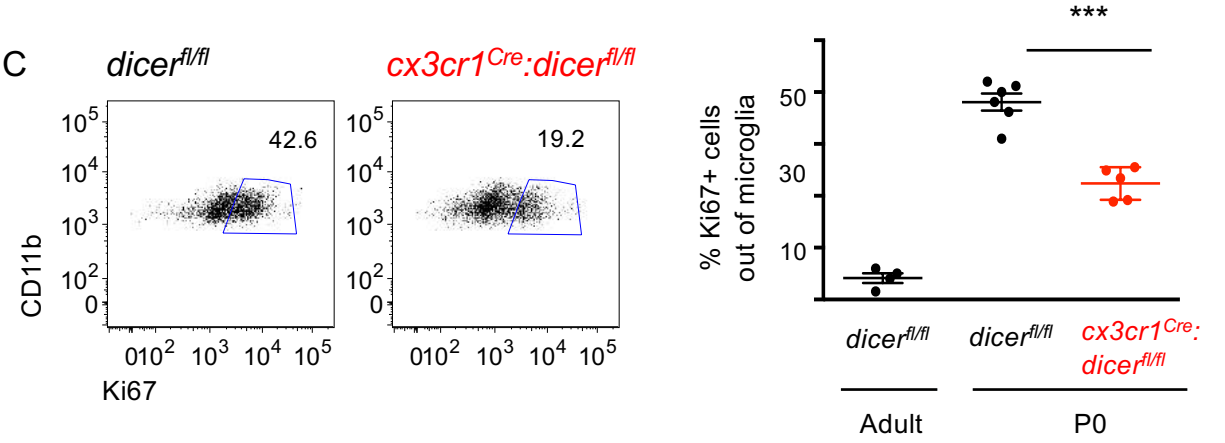

Varol et al., Figure S6

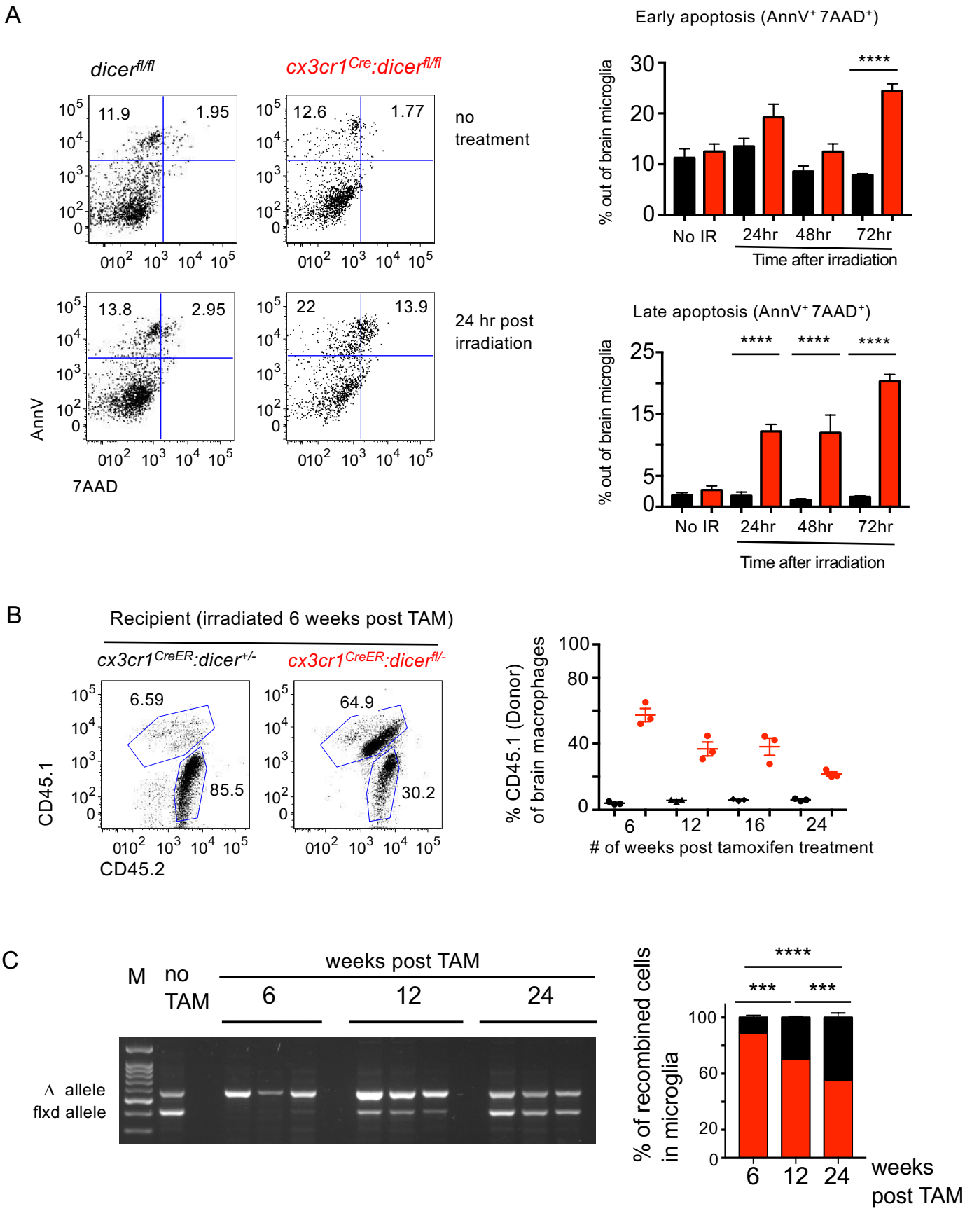

Varol et al., Figure S7

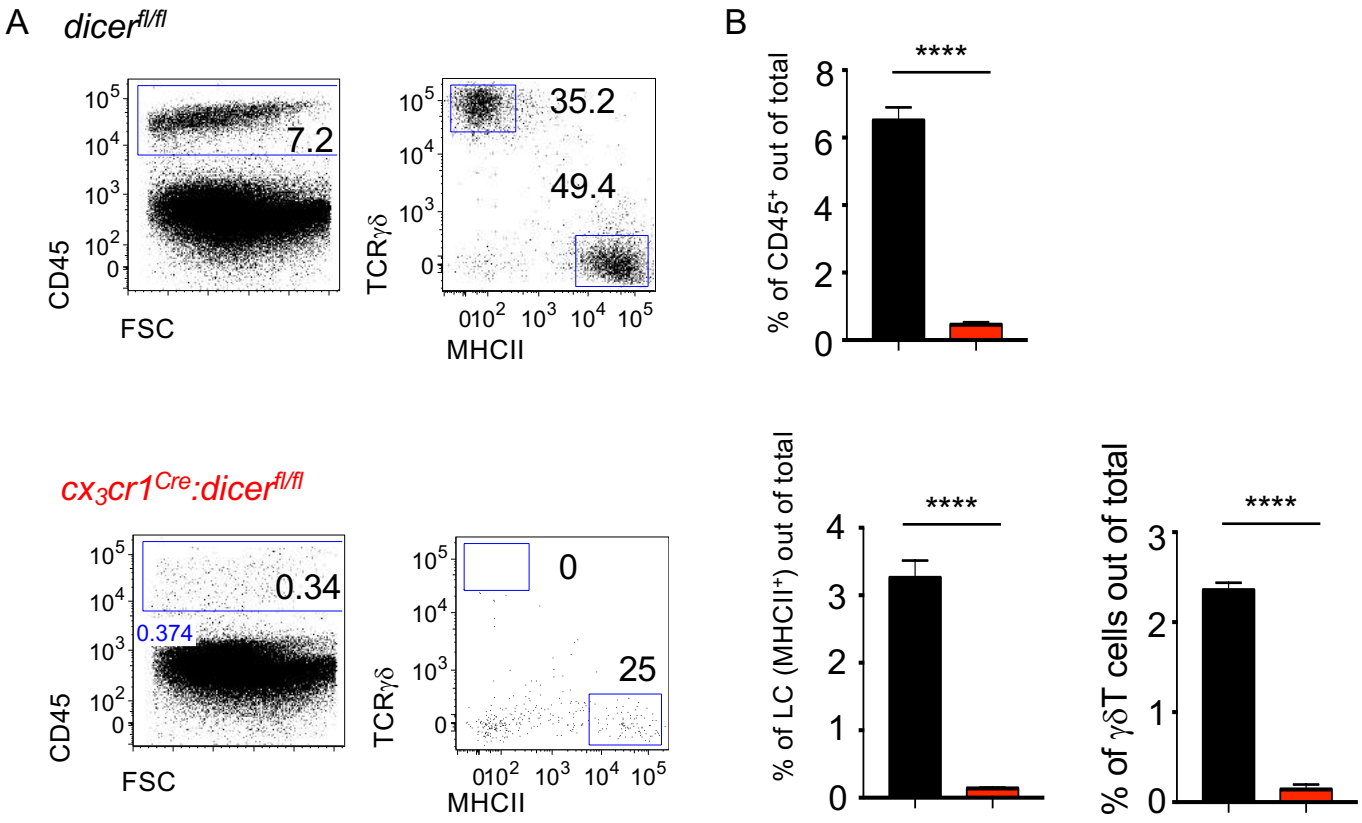

Varol et al., Figure S8

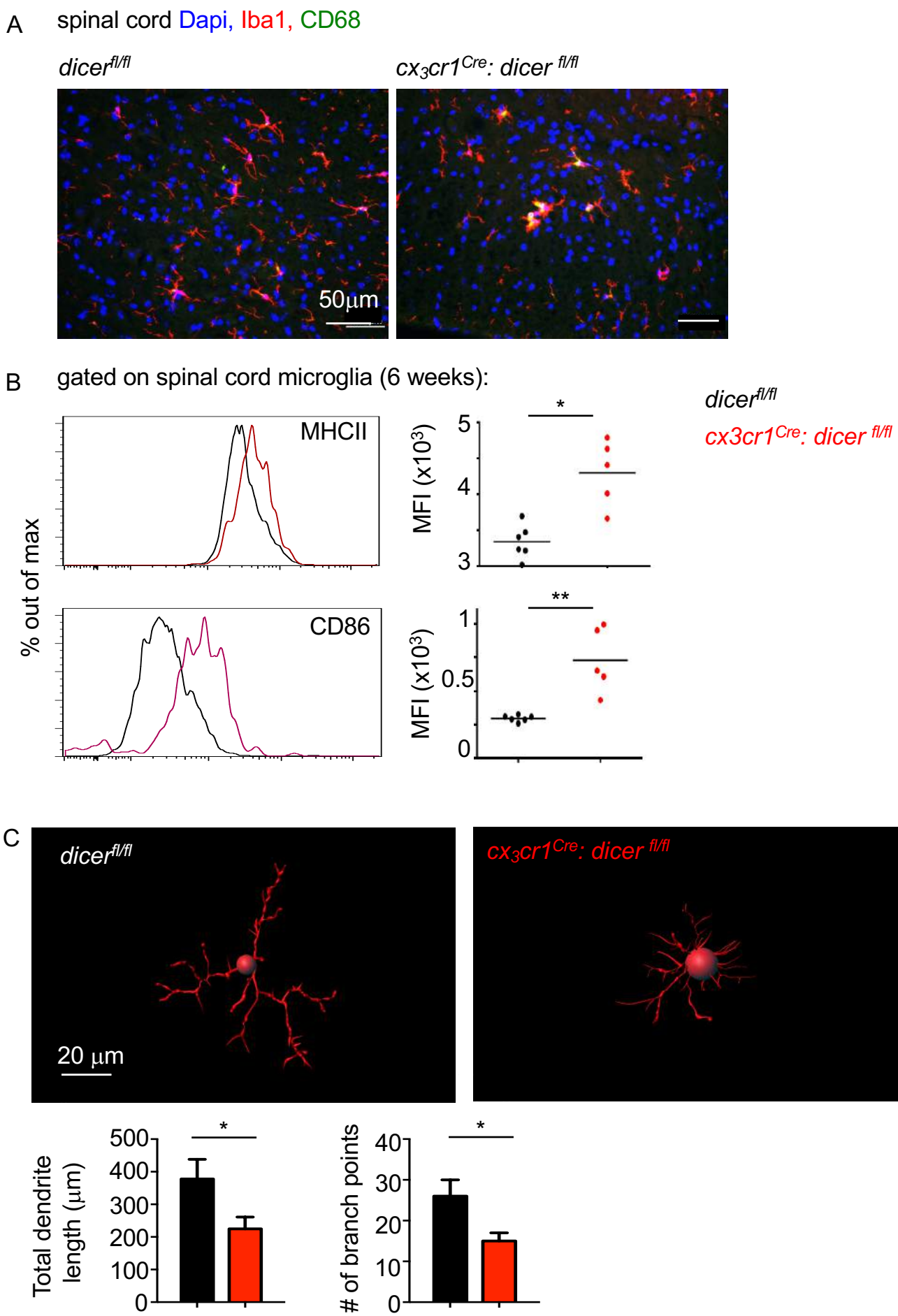

Varol et al., Figure S9

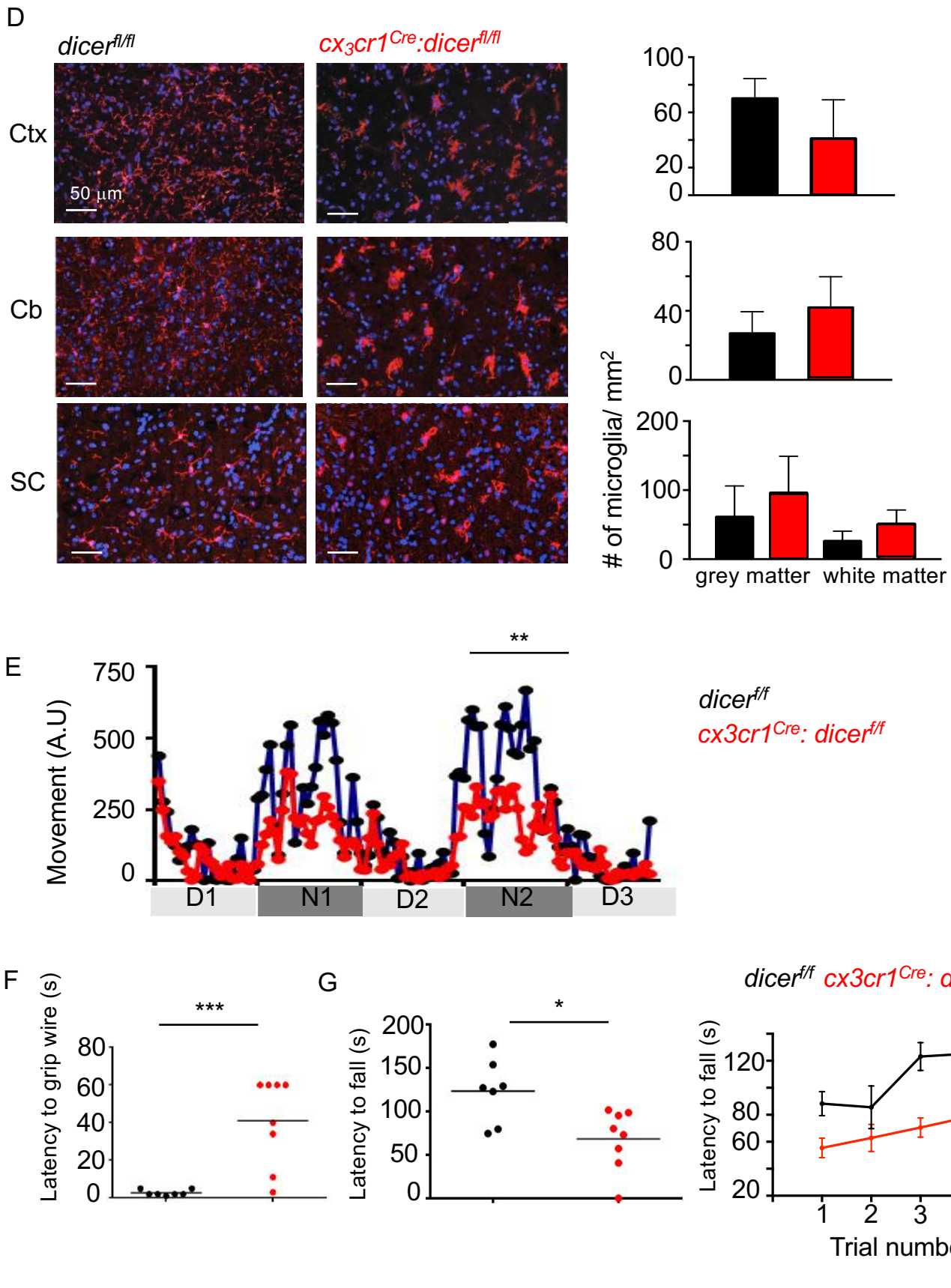

Varol et al., Figure S9

Click here to download Supplemental Text & Figures Varol et al 2nd revision Supplement text 12012017 final.docx

Varol et al. Online Supplement

Supplementary Figure 1

(A) Flow cytometry gating strategy for isolation of microglia, Kupffer cells (KC) and colonic macrophages.

(B) List of normalized, log2 transformed mean intensity values, representing the expression of miRNAs enriched in microglia compared with KC and colonic macrophages (displayed in Figure 1A, cluster I).

(C) List of normalized, log2 transformed, mean intensity values representing the expression of miRNAs mutually and highly expressed in microglia, KC and colonic macrophages. (intensity level >7, Agilent microarray). n=2 for each of the three macrophage subtypes (all differentially expressed miRNAs are displayed as a heat map in **Figure 1A**).

Supplementary Figure 2

(A) Representative two-photon *in vivo* images of microglia over a time-period of five minutes. The images of time-point 0 and 5 min were overlaid (Δt 5 min) to visualize stable (white), gained (green) and lost microglia processes (magenta).

(B) Turnover rate (TOR) of microglia processes as measured in *cx3cr1^{CreER}:dicer$^{fl/-}$:r26-YFP* and *Cx3cr1^{CreER}:dicer $^{+/-}$:r26-YFP* mice. TOR was calculated as percent lost and gained (changed) area of the whole microglia occupying area within a time-period of 5 min. Data are expressed as mean +/- SEM statistically analyzed with a Student's T-test (**P<0.01). *cx3cr1^{CreER}:dicer$^{fl/-}$:r26-YFP* (n=4), c*x3cr1^{CreER}:dicer $^{+/-}$:r26-YFP* mice (n=6).

Supplementary Figure 3

(A) Graphical summary of significantly changed canonical pathways in microglia isolated from TAM-treated *cx3cr1^{CreER}:dicer^{fll-}* mice compared to controls, analyzed by ingenuity pathway analysis (P value (pathway enrichment score)<0.05, Zscore (pathway activation score) >1.5).

(B) Graphical summary of significantly enriched Go annotations for biological process in microglia isolated from TAM-treated *cx3cr1^{CreER}:dicer^{fll-}* mice compared to controls (P value (pathway enrichment score)<0.05).

cx3cr1^{CreER}*:dicer*$^{+/-}$ (n=4), *cx3cr1*^{CreER}*:dicer*$^{fl/-}$ (n=3).

Supplementary Figure 4

(A) Table summarizing the significantly enriched Go annotations for biological processes associated with heat map clusters of differentially expressed genes of microglia isolated either 6hr post PBS or LPS *i.p* injection of *cx3cr1*^{CreER}*:dicer*$^{fl/-}$ and control mice (see **Figure 4A)**. Enriched Go annotations were found for clusters I, IV, VII and VIII.

(B) Table listing 10 miRNAs predicted by GSEA enrichment score test and a hyper geometric test to target the genes increased in microglia isolated from TAM-treated *cx3cr1*^{CreER}*:dicer*$^{fl/-}$ mice compared with control mice following LPS challenge (see **Figure 4A**, clusters IV and V).

(C) Graphical display of GSEA enrichment score histograms for miRNAs listed in **Figure S4B**. Replicate number (A-C): *cx3cr1*^{CreER}*:dicer*$^{+/-}$ PBS mice (n=3), *cx3cr1*^{CreER}*:dicer* $^{+/-}$ LPS mice (n=4), *cx3cr1*^{CreER}*:dicer*$^{fl/-}$ PBS mice (n=3), and *cx3cr1*^{CreER}*:dicer*$^{fl/-}$ LPS mice (n=4).

(D) Graphical summary of qRT-PCR analysis showing relative quantities of mRNA for *il1b, il18rap and fn1* in microglia sorted from non-treated (NT), 6hr and 12hr post LPS *i.p* injection (top), or 6hr post poly I:C *i.p* injection (bottom) of TAM-treated *cx3cr1*^{CreER}*:dicer*$^{fl/-}$ and control mice. Data are expressed as mean ± SEM and statistically analyzed with one-way ANOVA for multiple comparisons (*P<0.05, **P<0.01). *cx3cr1*^{CreER}*:dicer*$^{+/-}$ NT (n=3), *cx3cr1*^{CreER}*:dicer*$^{fl/-}$ NT (n=3), *cx3cr1*^{CreER}*:dicer*$^{+/-}$ 6hr LPS (n=4), *cx3cr1*^{CreER}*:dicer*$^{fl/-}$ 6hr LPS (n=3), *cx3cr1*^{CreER}*:dicer*$^{+/-}$ 12hr LPS (n=3), *cx3cr1*^{CreER}*:dicer*$^{fl/-}$ 12hr LPS (n=3), *cx3cr1*^{CreER}*:dicer*$^{+/-}$ 6hr poly I:C (n=3), *cx3cr1*^{CreER}*:dicer*$^{fl/-}$ 6hr poly I:C (n=3).

Supplementary Figure 5

(A) Graphical heat map display of mRNA profiles of hippocampal microglia isolated 6hr post PBS- or LPS-injection of TAM-treated *cx3cr1*^{CreER}*:dicer*$^{fl/-}$ and control mice. Genes displayed represent a fold change of at least 2 between any two of the groups (1339 genes). Normalized read numbers were log-transformed and standardized. Genes were clustered by a Pearson correlation test, number of partition clusters was set to eight. *cx3cr1*^{CreER}*:dicer*$^{+/-}$ PBS mice (n=2), *cx3cr1*^{CreER}*:dicer*$^{+/-}$ LPS mice (n=2), *cx3cr1*^{CreER}*:dicer*$^{fl/-}$ PBS mice (n=3) and *cx3cr1*^{CreER}*:dicer*$^{fl/-}$ LPS mice (n=2).

(B) Examples of gene expression as identified in cluster III (A). Shown are mean sequence reads ± SEM.
(C) Graphical summary of fiber volley and excitatory post synaptic potential (EPSP) as a function of stimulation intensity in hippocampal slices isolated from TAM-treated *cx3cr1*^{CreER}*:dicer*$^{fl/-}$ and *cx3cr1*^{CreER}*:dicer*$^{+/-}$ mice 12hr post PBS, 12hr post LPS and 24hr post LPS (1mg/Kg) i.p injection (related to **Figure 5F)**. *cx3cr1*^{CreER}*:dicer* $^{+/-}$ PBS, 12 hr, 24hr LPS (n=4 each); *cx3cr1*^{CreER}*:dicer*$^{fl/-}$ PBS (n=3), 12 hr (n=4), 24hr LPS (n=4).
(D) LTP analysis on Schaffer collateral *cornu ammonis* 1 (CA1) region synapses probed in acute hippocampal slices isolated from either 12hr post PBS, 12hr post LPS or 24hr post LPS treated *cx3cr1*^{CreER}*:dicer*$^{fl/-}$(red), littermate controls (blue) and C57BL/6 WT (black) mice. Averaged EPSP are plotted versus time. Data are expressed as mean +/- SEM and statistically analyzed with two way ANOVA on time point 60 considering the type of treatment, genotype and the interaction between the two factors. (*P<0.05, **P<0.01 represent the significance of interaction). Representative traces at indicated times (a,b) are shown on top of each section. Upward arrows indicate the time of high-frequency stimulation (HFS). *cx3cr1*^{CreER}*:dicer*$^{+/-}$ PBS, 12 hr LPS, 24hr LPS (n=4 each); *cx3cr1*^{CreER}*:dicer*$^{fl/-}$ PBS, 12 hr LPS, 24hr LPS (n=3 each); WT PBS, 12 hr LPS, 24hr LPS (n=3 each).

Supplementary Figure 6

(A) Graphical summary of significantly changed canonical pathways in microglia isolated from P0 *cx3cr1*^{Cre}*:dicer*^{fllfl} mice compared with controls (related to **Figure 6E**), analyzed by ingenuity pathway analysis (P value (pathway enrichment score)<0.05 and Abs[Zscore] (pathway activation score) >1.5), including increased (orange) and decreased (blue) pathways. *cx3cr1*^{Cre}*:dicer*$^{fl/fl}$ (n=2), *dicer*$^{fl/fl}$ mice (n=3).
(B) Gating strategy for the expression of nuclear proliferation marker Ki67 based on flow cytometric analysis of newborn and adult microglia of C57BL/6 WT mice.
(C) Flow cytometric analysis of microglia isolated from adult *dicer*$^{fl/fl}$, P0 *dicer*$^{fl/fl}$ and P0 *cx3cr1*^{Cre}*:dicer*$^{fl/fl}$ mice for the expression of the nuclear proliferation marker Ki67, including graphical summary (right). Data are expressed as mean +/- SEM and statistically analyzed with student's T test (***P<0.001); adult *dicer*$^{fl/fl}$ (n=4), P0 *dicer*$^{fl/fl}$ (n=6) and P0 *cx3cr1*^{Cre}*:dicer*$^{fl/fl}$ (n=5)

Supplementary Figure 7

(A) Representative plots of FACS analysis (left) and a graphical summary (right) of the frequencies for early and late apoptotic microglia of adult *cx3cr1^{Cre}:dicer$^{fl/fl}$* and *dicer$^{fl/fl}$* mice, untreated or 24hr, 48hr, and 72hr following irradiation. Data are represented as mean +/- SEM and statistically analyzed with one-way Anova for multiple comparisons (****P<0.0001); n=3 per group.

(B) Representative plots of FACS analysis (left) and graphical summary (right) of brain macrophage distribution between donor and recipient cells isolated from [*cx3cr1$^{gfp/+}$* (*CD45.1) > cx3cr1^{CreER}:dicer$^{+/-}$*] and [*cx3cr1$^{gfp/+}$* (*CD45.1) > cx3cr1^{CreER}:dicer$^{fl/-}$*] BM chimeras. Recipient mice were irradiated and BM transferred 6 (shown in representative FACS plot), 12, 16, and 24 weeks post TAM treatment (see **Figure 1A** for the preparation and analysis of TAM treated *cx3cr1^{CreER}:dicer$^{fl/-}$* mice). Brain macrophage contributions of donor (CD45.1) and recipient (CD45.2) were measured 6 weeks after transplantation. Note that the longer the gap between TAM treatment and irradiation, the lower the percentage of microglia replacement by BM graft derived cells. Data are represented as mean +/- SEM; n=3 per group.

(C) Genomic PCR image (left) and a graphical summary (right) measuring the ratio of floxed and recombined *dicer* alleles in sorted brain microglia from *cx3cr1^{CreER}:dicer$^{fl/-}$* mice and controls, 6 12 and 24 weeks post TAM treatment given at 4 weeks of age. Data are represented as mean +/- SEM; n=3 per group.

Supplementary Figure 8

(A) Representative plots of FACS analysis of epidermis from 6-8 week old *dicer$^{fl/fl}$* and *cx3cr1^{Cre}:dicer$^{fl/fl}$* mice indicating absence of Langerhans cells (LC) and dermal epithelial T cells (DETC).

(B) Graphical summary of data presented in (A). Data are expressed as mean +/- SEM; *dicer$^{fl/fl}$* (n=3) and *cx3cr1^{Cre}:dicer$^{fl/fl}$* mice (n=6).

Supplementary Figure 9

(A) Representative fluorescent microscopic images of frozen sections of SC tissues of 6 weeks old *cx3cr1^{Cre}:dicer$^{fl/fl}$* and control mice; Iba1 (red), CD68 (green) and Dapi (blue).

(B) Representative flow cytometry analysis for MHC II and CD86 expression of microglia of *cx3cr1^{Cre}:dicer$^{fl/fl}$* and control mice (left) and graphical summary of MFI of

staining (right). Data are expressed as mean +/- SEM. Statistical analysis was performed with Student's T test (*P<0.05, **P<0.01). *dicer*$^{fl/fl}$ (n=6), *cx3cr1*^{Cre}*:dicer*$^{fl/fl}$ (n=5).

(C) Representative three-dimensional Imaris-based reconstruction of spinal cord microglia morphology (top) and a graphical summary for morphological changes (bottom) of *cx3cr1*^{Cre}*:dicer*$^{fl/fl}$ mice and *dicer*$^{fl/fl}$ controls. Each symbol represents an average of at least three cells measured in a specific tissue sample. Data are expressed as mean +/- SEM. Statistical analysis was performed with Student's T test (*P<0.05); *dicer*$^{fl/fl}$ (n=5), *cx3cr1*^{Cre}*:dicer*$^{fl/fl}$ (n=4).

(D) Representative fluorescent microscopic images of paraffin sections from motor cortex, cerebellum and SC tissues of 8 week old *cx3cr1*^{Cre}*:dicer*$^{fl/fl}$ and *dicer*$^{fl/fl}$ mice, Iba1 (red), Dapi (blue) (left); and a graphical summary (right) of microglia densities in the respective CNS areas, including SC grey and white matter regions. Data are represented as mean +/- SEM and statistically analyzed with Student's T test (NS P>0.05); n=5 per group.

(E) Graphical summary of home-cage locomotion assay performed on 8 week old *cx3cr1*^{Cre}*:dicer*$^{fl//fl}$ and *dicer*$^{fl//fl}$ mice. Data are represented as average activity per group for each time point, statistically measured with repeated measure Student's T test (**P<0.01); n=6 per group.

(F) Graphical summary of hang-wire test performed on 8 week old *cx3cr1*^{Cre}*:dicer*$^{fl//fl}$ and *dicer*$^{fl//fl}$ mice. Data are represented as mean +/- SEM and statistically analyzed with Student's T test (*** P<0.001); *dicer*$^{fl//fl}$ (n=8) and *cx3cr1*^{Cre}*:dicer*$^{fl//fl}$ (n=7).

(G) Graphical summary of rotarod spinning wheel test (left) and of training (trial 1 and 2) together with measurement (trial 3, 4 and 5) (right) of rotarod spinning wheel test performed on 8 week old *cx3cr1*^{Cre}*:dicer*$^{fl//fl}$ and *dicer*$^{fl//fl}$ mice.

Data are represented as mean +/- SEM, statistically measured with Student's T test (*P<0.05); *dicer*$^{fl//fl}$ (n=8) and *cx3cr1*^{Cre}*:dicer*$^{fl//fl}$ (n=7).